

Fluorescently Labeled Latex Particles to Monitor Film Formation

by

Victoria Hisko

A thesis

presented to the University of Waterloo

in fulfilment of the

thesis requirement for the degree of

Master of Science

in

Chemistry

Waterloo, Ontario, Canada, 2017

© Victoria Hisko 2017

Author's Declaration

I hereby declare that I am the sole author of this thesis. This is a true copy of the thesis, including any required final revisions, as accepted by my examiners.

I understand that my thesis may be made electronically available to the public

Abstract

The influence of the length of an oligo(ethylene glycol) spacer (EG_n , where n is the number of ethylene glycol units) in a 1-pyrenemethoxy- EG_n methacrylate (PyEG-MA) monomer on the incorporation of the monomer into a poly(n -butyl methacrylate) (PBMA) latex and on the diffusion of the pyrene-labeled PBMA (PyEG _{n} -PBMA) in latex films was investigated. The PyEG _{n} -MA monomers were prepared by two different methods. The anionic polymerization of ethylene oxide, using potassium 1-pyrenemethoxide as initiator, yielded ethoxylated 1-pyrenemethanol that was reacted with methacrylic anhydride to yield the PyEG _{n} -MA monomer. Alternately, monotosylated well-defined ethylene glycol oligomers were successively coupled with 1-pyrenemethoxide and methacrylic anhydride. The monomers were copolymerized with n -butyl methacrylate by emulsion polymerization. A longer $\text{EG}_{7.4}$ spacer was found to enhance the incorporation of the PyEG_{7.4}MA monomer up to 3.2 mol%, substantially higher than 1.9 mol% achieved previously with an EG_3 spacer. The higher incorporation of PyEG_{7.4}MA into the Py-PBMA latex led to a stronger pyrene excimer fluorescence (PEF) signal in the spectrum of the latex film. The goal was to use these fluorescently labeled particles to probe interparticle polymer diffusion (IPD) during film formation.

Several issues arose in the copolymerization of PyEG_{7.4}MA and n -butyl methacrylate (BMA). The aggregation of PyEG_{7.4}MA into flower-like micelles was observed. Even though steps were taken to mitigate this effect in the emulsion polymerization process, the pyrene molecules tended to be more concentrated near the surface of the latex particles. This resulted in irreproducible annealing results, and it is recommended that these particles not be employed for the study of IPD.

Acknowledgements

I would like to acknowledge my supervisors, Professors Mario Gauthier and Jean Duhamel, for welcoming me to academia and for their ongoing support throughout this project.

I would like to thank all the members of the Gauthier and Duhamel labs – time flew with you as labmates! I would specifically like to thank Remi Casier for initiating the project and for guidance throughout, and Joanne Fernandez for her friendship, support and apples.

Finally, I would like to thank BASF and NSERC for funding support.

Table of Contents

List of Figures.....	vii
List of Schemes.....	x
List of Tables.....	xi
List of Abbreviations.....	xii
<i>Chapter 1: Introduction</i>	1
1.1 Background.....	1
1.2 Synthesis of the Latex Particles.....	3
1.2.1 Batch Emulsion Polymerization.....	3
1.2.1.1 Particle Nucleation by Micellar Nucleation.....	4
1.2.1.2 Particle Nucleation by Homogenous Nucleation.....	4
1.2.1.3 Monomer Droplet Initiation.....	4
1.2.1.4 Coagulative Nucleation.....	6
1.2.1.5 The Second and Third Stages.....	6
1.2.2 Copolymerization and Reactivity Ratios.....	7
1.2.3 Semi-Batch Emulsion Polymerization.....	9
1.3 Methods to Probe IPD.....	10
1.3.1 Small-Angle Neutron Scattering (SANS).....	10
1.3.2 Förster Resonance Energy Transfer (FRET).....	12
1.3.3 Pyrene Excimer Fluorescence (PEF).....	16
1.4 Thesis Outline.....	19
<i>Chapter 2: Monomer Synthesis</i>	22
2.1 Materials.....	22
2.2 Instrumentation.....	24
2.3 Synthesis of PyLMs.....	25
2.3.1 Synthesis of Ethoxylated 1-Pyrenemethanol (PyEG _n OH).....	25
2.3.1.1 Coupling of Oligo(Ethylene Glycol) Segments with 1-Pyrenemethanol.....	25
2.3.1.2 Synthesis of PyEG _n OH by Anionic Polymerization.....	27

2.3.2 Methacrylation of Ethoxylated 1-Pyrenemethanol.....	28
2.4 Characterization of PyLMs.....	29
2.5 Aggregation of PyLM in Aqueous Solution.....	33
2.6 Summary.....	35
<i>Chapter 3: Particle Synthesis and Characterization.....</i>	<i>36</i>
3.1 Synthesis of Latex Particles.....	36
3.3.1 Addition of Dodecanethiol.....	38
3.2 Characterization of the Latex Particles.....	39
3.3 Polymerization Issues.....	43
3.3.1 Aggregation.....	43
3.3.2 Pyrene Cleavage.....	47
3.4 Summary.....	47
 <i>Chapter 4: Film Formation.....</i>	 <i>49</i>
4.1 Experimental.....	50
4.2 Steady-State Fluorescence.....	51
4.2.1 Photobleaching.....	54
4.2.2 Other Complications Encountered in the Characterization of IPD by Steady-State Fluorescence.....	57
4.2.3 Film Color Change.....	63
4.3 Summary.....	65
 <i>Chapter 5: Summary and Discussion.....</i>	 <i>66</i>
 <i>References.....</i>	 <i>69</i>

List of Figures

<i>Figure 1-1:</i> Film formation process for latex particles.....	2
<i>Figure 1-2:</i> Homogenous nucleation process for emulsion polymerization.....	5
<i>Figure 1-3:</i> The emulsion polymerization process.....	7
<i>Figure 1-4:</i> Diagram showing the mixing of the donor- and acceptor-labeled polymers before and after film formation.....	13
<i>Figure 1-5:</i> Jablonski diagram describing the fluorescence process.....	13
<i>Figure 1-6:</i> Top: Kinetic scheme representing pyrene excimer formation through encounters between an excited and a ground-state pyrene. Bottom: Resulting steady-state fluorescence spectrum.....	17
<i>Figure 1-7:</i> Change in distribution of pyrene labels in a latex film during film formation from (left) when the particles have deformed but no IPD has taken place to (right) a fully annealed film.	18
<i>Figure 2-1:</i> Diagram of an ampule (left) and vacuum line manifold (right)	27
<i>Figure 2-2:</i> 300 MHz ¹ H NMR spectra in CDCl ₃ for PyEG _{7.4} OH and the corresponding PyLM in CDCl ₃ . Top: δ 8.0-8.4 (m, 9 H), 5.3 (s, 2 H), 3.4- 3.9 (m, 29.6 H). Bottom: δ 8.0-8.4 (m, 9 H), 6.1 (s, 1H) 5.5 (s, 1 H), 4.2 (m, 2 H), 5.3 (s, 2 H), 3.4- 3.9 (m, 27.6 H), 1.9 (s, 3 H). Residual solvent peaks are present at δ 7.2 ppm for CHCl ₃	30
<i>Figure 2-3:</i> DRI and UV-Vis traces for PyEG ₇ MA.....	31
<i>Figure 2-4:</i> Steady-state fluorescence spectra (left) and time-resolved fluorescence decays (right) of ethoxylated 1-pyrenemethanol (<i>n</i> = 7.4) (top) with $\chi^2 = 1.00$, and the corresponding PyLM (bottom) with $\chi^2 = 1.10$	32
<i>Figure 2-5:</i> Left – Aqueous solution of PyEG ₄ MA, showing a single hydrophobic bead at the bottom of the vial. Right – Aqueous dispersion of PyEG _{7.4} MA at the same concentration.....	33
<i>Figure 2-6:</i> Time-resolved excimer fluorescence decays for 5 mM PyEG _{7.4} MA in A) THF and B) water; $\lambda_{\text{ex}} = 344$ nm, $\lambda_{\text{em}} = 510$ nm.....	34
<i>Figure 3-1:</i> Three-neck reaction vessel used for emulsion polymerization. A condenser was fitted on Side A of the reactor and a rubber septum on Side B.....	37

<i>Figure 3-2:</i> DRI GPC traces for copolymers synthesized at different CTA concentrations. Blue: Monomer, Black: [CTA] = 0 mg/g, [I] = 5 mg, Yellow: [CTA] = 0.3 mg/g, [I] = 3.5 mg, Red: [CTA] = 2.5 mg/g, [I] = 6.5 mg, Orange: [CTA] = 10 mg/g, [I] = 5.5 mg. 5% PyEG _{7,4} MA was used in all syntheses except for the 0 mg/g trial where 2% PyLM was used to minimize crosslinking as a molecular weight baseline.....	39
<i>Figure 3-3:</i> GPC traces for the unlabelled <i>n</i> -butyl methacrylate homopolymer and PyEG _{7,4} -PBMA(3.2).....	40
<i>Figure 3-4:</i> DSC profile for PyEG _{7,4} -PBMA(3.2) showing T _g = 20°C.....	41
<i>Figure 3-5:</i> Fluorescence spectrum for PyEG _{6,5} -PBMA(2.8)	43
<i>Figure 3-6:</i> Time-resolved fluorescence decays for copolymers synthesized via solution and emulsion polymerization, with respective residuals and autocorrelation functions. Emulsion copolymerization yielded a steeper decay in the monomer, corresponding to more clustered pyrene molecules.	45
<i>Figure 4-1:</i> Steady-state fluorescence spectra for A) PyEG ₃ -PBMA(1.9)labeled and B) 2.8% PyEG _{6,5} -PBMA(2.8)-labeled films at T = 100°C at different annealing times.....	53
<i>Figure 4-2:</i> Fraction of mixing as a function of annealing time at T = 90 °C for (■) PyEG _{6,5} -PBMA(2.8) (230 kg/mol), (▲) PyEG ₃ -PBMA(1.9) (430 kg/mol), and (●) PyEG ₃ -PBMA(1.9) (200 kg/mol). PyEG _{6,5} -PBMA(2.8) is seen to diffuse much more quickly in the first 2 hours of annealing.....	54
<i>Figure 4-3:</i> Latex films (5% PyEG _{7,4} -PBMA(3.2), 95% native PBMA) cast on a quartz plate and irradiated for different time periods in the fluorometer. The films were excited with a hand-held UV lamp and photographed either as-is (top) or through a 495 nm cut-off filter (bottom). The bleached rectangular area visible at the center of the film corresponds to the zone irradiated by the lamp of the fluorometer.....	55
<i>Figure 4-4:</i> Plot of the I _E /I _M ratio normalized to t _{an} = 0 as a function of irradiation time. The latex film (5% PyEG _{7,4} -PBMA(3.2), 95% native PBMA) was cast (left) on a quartz plate and (right) on the wall of a square quartz tube that was kept under nitrogen atmosphere.....	56
<i>Figure 4-5:</i> Fluorescence spectra for A) PyEG ₃ -PBMA(1.9) and B) PyEG _{6,5} -PBMA(2.8) latex particles at increasing concentrations of nitromethane. (C) Normalized fluorescence intensity of the pyrene monomer for (○) PyEG ₃ -PBMA(1.9) and (△) PyEG _{6,5} -	

PBMA(2.8) latex particles as a function of the nitromethane concentration.....	61
<i>Figure 4-6: Fluorescence spectra for the A) PyEG_{6,5}-PBMA(2.8) and B) PyEG₃-PBMA(1.9) latex particles normalized at 375 nm, (C) Normalized I_E/I_M ratio for (●) PyEG₃-PBMA(1.9) and (▲) PyEG_{6,5}-PBMA(2.8) latex particles as a function of the nitromethane concentration.</i>	
	62

List of Schemes

<i>Scheme 2-1: Synthesis of PyEG_nOH by coupling of oligo(ethylene glycol) with PyMeOH.....</i>	26
<i>Scheme 2-2: Synthesis of PyEG_nOH by anionic polymerization.....</i>	28
<i>Scheme 2-3: Reaction of PyEG_nOH with methacrylic anhydride.....</i>	29

List of Tables

<i>Table 3-1:</i> Characteristics of latexes prepared via emulsion copolymerization of <i>n</i> -BuMA and PyLM.....	42
<i>Table 3-2:</i> Parameters f_{agg} , $k_{\text{blob}} \times N_{\text{blob}}$, and $\langle \tau \rangle$ retrieved from the decay analysis.....	44
<i>Table 4-1:</i> I_E/I_M at $t_{\text{an}} = 0$ and $t_{\text{an}} = \infty$ obtained from fluorescence spectra acquired at three different spots on three films (5% PyEG _{6.5} -PBMA(2.8), 95% PBMA), annealed at three different temperatures.....	57
<i>Table 4-2:</i> Representative I_E/I_M values at $t_{\text{an}} = 0$ and 7 min at $T = 100^\circ\text{C}$, and decrease in I_E/I_M over the first 7 min and after complete mixing ($t_{\text{an}} = \infty$) for latex film (5% PyEG _{6.5} -PBMA(2.8) and 95% native PBMA).....	58
<i>Table 4-3:</i> Pictures for PyEG ₃ MA- and PyEG _{6.5} MA-labeled films annealed at 75°C and excited with long-wavelength UV light (no cut-off filter applied).....	63
<i>Table 4-4:</i> Pictures for PyEG ₃ MA- and PyEG _{6.5} MA-labeled films annealed at 75°C and excited with long-wavelength UV light (with 475 nm cut-off filter).....	64

List of Abbreviations

A	Acceptor
APS	Ammonium persulfate
AOT	Sodium docusate salt
BMA	<i>n</i> -Butyl methacrylate
C_{Py}	Local pyrene concentration
CMC	Critical micelle concentration
CTA	Chain transfer agent
D	Apparent diffusion coefficient
D	Donor
d	Mean diameter
D_h	Hydrodynamic diameter
DCM	Dichloromethane
DLS	Dynamic light scattering
DMF	<i>N,N</i> -Dimethylformamide
DMAP	Dimethylaminopyridine
DP	Degree of polymerization
DRI	Differential refractive index
DSC	Differential scanning calorimetry
E_{ET}	FRET efficiency
EG_n	Oligo(ethylene glycol)
f_x	Mole fraction of monomer in feed
F_x	Mole fraction of monomer in copolymer
f_{agg}	Molar fraction of aggregated pyrenes
F_D	Fluorescence intensity in absence of acceptor
F_{DA}	Fluorescence intensity in presence of acceptor
f_m	Corrected fraction of mixing
f'_m	Apparent fraction of mixing
FRET	Fluorescence resonance energy transfer
GPC	Gel permeation chromatography
I_E/I_M	Ratio of the fluorescence intensity of the pyrene excimer over that of the pyrene monomer
IPD	Interparticle polymer diffusion
$j_{critical}$	Critical length of oligomer
k	Rate constant
k_{blob}	Rate constant at which a pyrene label encounters another inside a blob
MFT	Minimum film formation temperature
M_n	Number-average molecular weight
M_w	Weight-average molecular weight

MWD	Molecular weight distribution
NMR	Nuclear magnetic resonance
PBMA	Poly(<i>n</i> -butyl methacrylate)
PDI	Polydispersity index
PEF	Pyrene excimer fluorescence
Py	Pyrene
PyEG _{<i>n</i>} MA	Pyrene-labelled monomer with an oligo(ethylene glycol) linker length having a degree of ethoxylation <i>n</i>
PyEG _{<i>n</i>} OH	Ethoxylated pyrenemethanol with degree of ethoxylation <i>n</i>
PyLM	Pyrene-labeled monomer
PyMeOH	Pyrenemethanol
Py-PBMA	Pyrene-labelled poly(<i>n</i> -butyl methacrylate)
<i>r</i>	Radius of a solid sphere
<i>R</i> ₀	Förster radius
<i>R</i>	Distance separating donor from acceptor
<i>R</i> _g	Radius of gyration
<i>r</i>	Reactivity ratio
SANS	Small-angle neutron scattering
<i>T</i> _{an}	Annealing temperature
<i>T</i> _g	Glass transition temperature
THF	Tetrahydrofuran
UV	Ultraviolet
λ_{ex}	Excitation wavelength
λ_{em}	Emission wavelength
σ	Standard deviation

Chapter 1

Introduction

1.1 Background

Paints and coatings are aqueous dispersions of colloids, most often petrochemical-based latex particles, which are applied onto surfaces as a thin layer. After water evaporation, the latex particles coalesce into a homogeneous film that, if properly designed, protects, embellishes or smoothens the underlying surface. Consequently, understanding the process of film formation is very important to the paint and coatings industry, as it will affect a number of film properties including surface hardness, adhesion, and toughness.^{1,2}

Film formation begins after a dispersion of latex particles has been applied onto a surface. The first step in the process is the formation of layers of close-packed particles following water evaporation.^{2,3} If the temperature is above the glass transition temperature of the polymer in the particles, these deform to fill any remaining voids, generating a honeycomb arrangement. At this stage, the film is weak and can crack along the boundaries of the particles. A film with good mechanical properties requires that the particles coalesce, as the constituting polymer chains cross the boundaries of the particles and undergo interparticle polymer diffusion (IPD).⁴ IPD leads to the

disappearance of the particle boundaries, thereby producing a homogenous film with desirable mechanical properties. The film formation process is depicted in Figure 1-1.

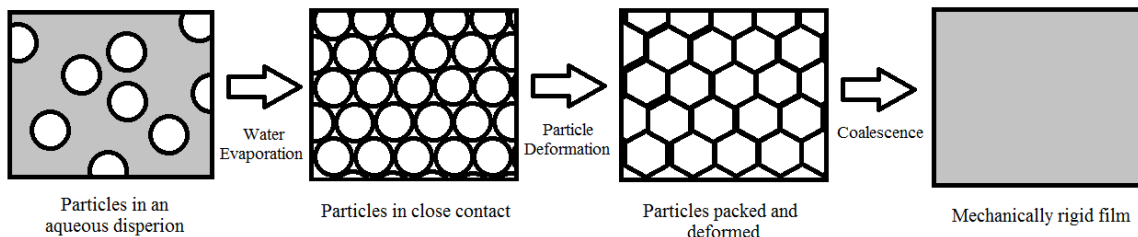


Figure 1-1: Film formation process for latex particles.

The conditions under which the film is formed will affect the rate of IPD and the performance of the film. For example, annealing must take place above the minimum film formation temperature (MFT) in order to produce a desirable, uniform film. Below the MFT, IPD will be limited and the film will appear fragile and powdery.

Due to the importance of the last step in Figure 1-1 to generate a homogeneous film, methods based on Förster Resonance Energy Transfer (FRET)⁵⁻⁸ and Small-Angle Neutron Scattering (SANS)⁹⁻¹¹ have been proposed to study IPD. However, these methods have a number of drawbacks and a new procedure based on pyrene excimer fluorescence (PEF) has been introduced recently that appears to yield the same quantitative information about IPD taking place in a latex film.¹² The procedure involves the synthesis of latex particles from a pyrene-labeled monomer, preparing a latex film with a mixture of the pyrene-labeled particles and non-fluorescent latex particles having otherwise similar properties as the fluorescently labeled ones, and monitoring the decrease in PEF as a function of annealing time. IPD leads to the dilution of the pyrene-labeled chains in the latex film, and the decrease in PEF can be used to determine the diffusion coefficient of the polymer in the film. While the PEF-based method shows impressive potential, an increase in the level of pyrene labeling of the fluorescent particles up from the value of 1.9 mol% already achieved¹² should facilitate the

detection of PEF and thus the characterization of IPD taking place in the film. The purpose of this thesis was to improve the synthetic procedure for the preparation of the pyrene-labeled latex to introduce a larger number of pyrene labels into the fluorescent particles, which would result in higher PEF. The synthetic strategy applied to prepare the pyrene-labeled particles, and the different techniques available to study latex film formation are reviewed hereafter.

1.2 Synthesis of Latex Particles

A latex is a dispersion of polymer particles, where the non-solvent used for the polymer is most commonly water. Dispersions are desirable due to their high polymer content, and since the polymerization can be carried out without organic solvents, they are popular for their environmentally friendly nature.^{13,14} The most widely used method to synthesize latex particles is emulsion polymerization, although subsets of emulsion polymerization such as mini- or microemulsion polymerization can also serve to synthesize latex particles from more hydrophobic monomers.¹⁵

1.2.1 Batch Emulsion Polymerization

Batch techniques are the simplest and most common form of emulsion polymerization. All the materials including the water, monomer, initiator, and surfactant are placed in the reactor prior to the reaction.¹⁶ There are three stages in the emulsion polymerization process: particle formation, particle growth, and completion of polymerization. The first stage, or particle formation, occurs through one or a combination of the following processes: micellar nucleation, homogenous nucleation, coagulative nucleation, or monomer droplet initiation. The specific mechanism(s) involved depend(s) on the properties of the different reaction components, but mainly on the hydrophilicity of the monomer. The main mechanisms of particle formation are described hereafter.

1.2.1.1 Particle Nucleation by Micellar Nucleation

Before starting the polymerization, a surfactant is added to the reactor above its critical micelle concentration (CMC). The surfactant forms micelles and the monomer phase separates into large droplets. The hydrophobic monomers partition themselves between the monomer droplets, the surfactant micelles, and the aqueous phase. The radical initiator, being water-soluble, reacts with the small amount of monomer present in the water phase. As the oligomer grows in length, it becomes more hydrophobic until it “stings” a monomer-swollen micelle, polymerizing any monomer within it and turning the micelle into a polymer particle. The surfactant molecules, initially forming the micelles, also stabilize the growing polymer particles.

1.2.1.2 Particle Nucleation by Homogenous Nucleation

The formation of latex particles has also been observed at surfactant concentrations below the CMC. In order to explain this phenomenon, the concept of homogenous nucleation was developed. Monomers which undergo homogenous nucleation are moderately soluble in water, such as methyl methacrylate. As in micellar nucleation, a water-soluble radical initiator is added to the polymerization vessel. A radical reacts with the monomer in the aqueous phase and the radical oligomer propagates until a critical length ($j_{critical}$) is reached, when the polymer becomes insoluble and is stabilized by adsorbing surfactant molecules, thus generating a new polymer particle.²⁴ From there on the polymer particle can solubilize monomer, capture growing oligomers, or further coagulate with other particles. This process is depicted in Figure 1-2.

1.2.1.3 Monomer Droplet Initiation

Monomer droplet initiation is the primary particle nucleation mechanism in certain types of polymerizations, namely mini- and microemulsions, which are a subset of emulsion polymerization that may be advantageous when the monomers are very hydrophobic. In a miniemulsion reaction

water, and the monomer, emulsifier and a co-stabilizer form two distinct phases. The main difference between conventional emulsion polymerization and miniemulsion systems, apart from the presence of a co-stabilizer, is the size of the droplets and its consequences on particle nucleation. Whereas monomer droplets with an initial diameter of 1 – 10 μm are created by mechanical stirring in conventional emulsion polymerization, the monomer droplets in a miniemulsion system are only 10 – 50 nm in diameter.²¹ The small droplet size is achieved through a high shearing force induced by either sonication or a mechanical homogenizer. In this context, +M in Figure 1-2 represents the addition of monomer units to a growing monomer chain, and α represents the fraction of chains whose length is above $j_{critical}$, which are captured by a particle.

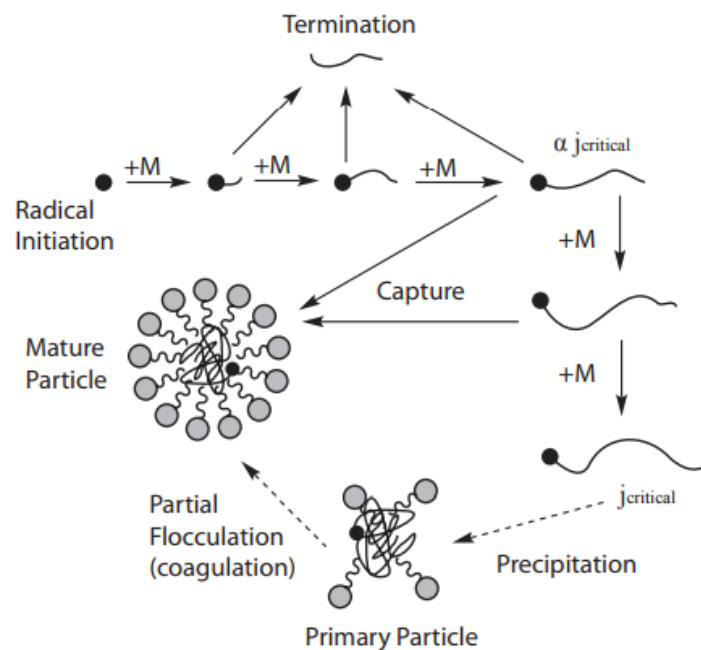


Figure 1-2: Homogenous nucleation process for emulsion polymerization.²⁴

Since the formation of smaller droplets requires more surfactant molecules, fewer micelles are present in the emulsion. The significantly smaller size of the droplets increases their surface area drastically, thus promoting radical entry into the monomer droplets. Consequently, droplet nucleation

through radical entry into the monomer droplets is the primary particle nucleation process in miniemulsions.

1.2.1.4 Coagulative Nucleation

Particle growth in the first stage eventually reduces the repulsive forces between particles, to the point where they are overcome by van der Waals attractive forces. This situation results in the aggregation and merger of polymer particles, also referred to as coagulative nucleation. This process reduces the surface area of the particles and restores the repulsive forces between particles, until further particle growth results in further coagulation. Eventually, mature polymer particles are generated.

1.2.1.5 The Second and Third Stages

Once coagulative nucleation stops and the number of particles in the reaction remains constant, the second phase of the process begins. The second stage of emulsion polymerization corresponds to particle growth occurring with a set number of polymer particles. The monomer diffuses out of the large monomer droplets, to reach the polymer particles where polymerization takes place. The disappearance of the large monomer droplets signals the end of the second stage.

In the third and final stage, the monomer remaining inside the particles is consumed. Once all remaining monomer is consumed, the polymerization is complete. The entire emulsion polymerization process is described in Figure 1-3.

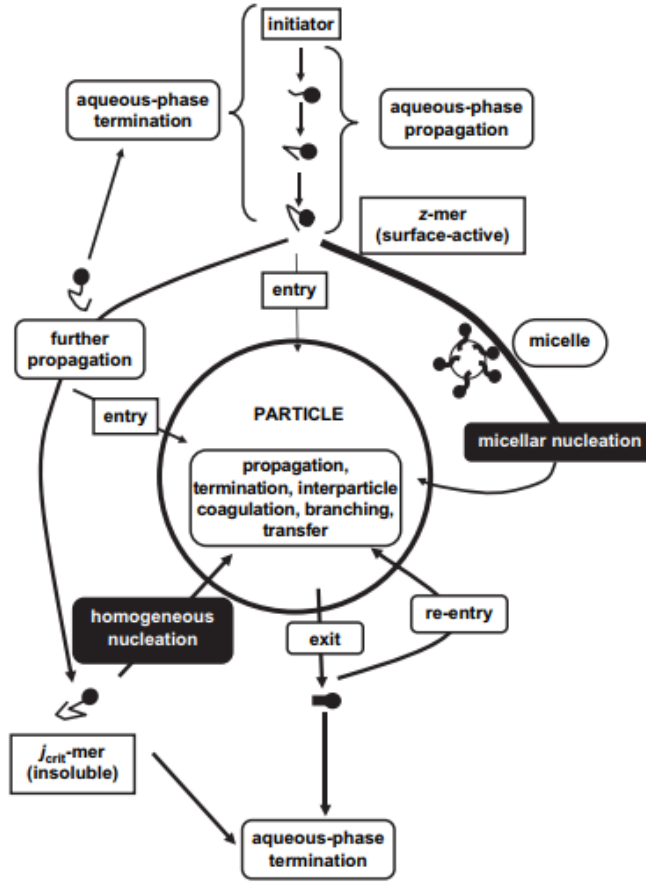


Figure 1-3: The emulsion polymerization process.²⁸

1.2.2 Copolymerization and Reactivity Ratios

Copolymerization can yield different kinds of polymers including alternating, random, and blocky copolymers.²⁹ The reactivity ratios in a binary copolymerization reaction can be used to predict the type of polymerization taking place, the monomer sequence distribution, and the rate of polymerization. Most commonly, propagation is assumed to depend solely on the last monomer addition. This is referred to as the terminal model.³⁰ For two monomers, homo- and cross-propagation reactions described by Equations 1-1 can occur:



The rate constants for each possible propagation step are defined as k_{11} , k_{12} , k_{22} , and k_{21} , respectively. The reactivity ratio for the first monomer would then be described as $r_1=k_{11}/k_{12}$, and as $r_2=k_{22}/k_{21}$ for the second monomer.¹⁷ The product of the reactivity ratios provides information about the type of copolymerization behavior, with $r_1 \times r_2$ values of 1, 0, or ∞ indicating ideal, alternating, or blocky copolymerization reactions, respectively.

One of the most widely used copolymerization models is the terminal model, otherwise known as the Mayo-Lewis model, which results in the Mayo-Lewis equation. There are two popular versions of this equation, represented by both Equations 1-2 and 1-3.^{29,31}

$$\frac{d[M_1]}{d[M_2]} = \left(\frac{[M_1]}{[M_2]} \right) \frac{r_1[M_1] + [M_2]}{[M_1] + r_2[M_2]} \quad (1-2)$$

$$F_1 = \frac{(r_1 - 1)f_1^2 + f_1}{(r_1 + r_2 - 2)f_1^2 + 2(1 - r_2)f_1 + r_2} \quad (1-3)$$

In the above equations, $[M_x]$ represents the feed concentration of monomer x , and F_x and f_x are the mole fractions of monomer x in the copolymer and in the feed, respectively. Equations 1-2 and 1-3 relate the feed composition to the copolymer composition. Compositional drift occurs when the cumulative and instantaneous molar fraction F_x are not the same for the copolymer. For this reason,

the Mayo-Lewis model may only be used when copolymerization reactions are run at low conversion, where compositional drift remains negligible.

The situation is more complicated in heterogeneous copolymerization reactions such as for emulsion copolymerization, since the relative rates of incorporation of the monomers into the copolymer depend not only on the intrinsic reactivity of the monomers, as described by Equations 1-2 and 1-3, but also on their solubility and diffusion coefficient in the water phase. In that case, different strategies may be necessary to ensure uniform incorporation of the monomers, such as using a semi-batch copolymerization process.

1.2.3 Semi-Batch Emulsion Polymerization

Semi-batch emulsion copolymerization has some advantages over traditional batch emulsion copolymerization, especially when one monomer is more reactive or more hydrophobic than the other. Batch emulsion copolymerization can suffer from compositional drift, which influences the chemical composition of the copolymer chains produced over the course of the reaction. In order to have a latex with predictable and desirable properties, chemical composition homogeneity must be controlled. Composition control and uniformity of the monomer distribution among the copolymer chains can be achieved successfully by semi-batch emulsion processes in many cases.

Semi-batch emulsion polymerization differs from batch emulsion polymerization in that only a portion of the materials is added to the reactor at the beginning of the reaction. In a typical semi-batch reaction the water, initiator and surfactant are first added to the reaction vessel, and the monomer mixture (either pure or pre-emulsified) is fed to the reactor over the course of the reaction. If the rate of monomer addition to the reactor is greater than the rate of polymerization, the polymerization occurs in a “flooded” state. In the case where the rate of addition is lower than the rate of polymerization, a “starved” state is created, where the rate of polymerization is controlled by

the feeding rate of the monomer.¹⁸⁻¹⁹ To create a starved state the monomer feeding rate must therefore be relatively slow, resulting in longer reaction times. To remedy this problem, it has been proposed that similar results may be obtained by feeding the more reactive monomer into a reaction vessel containing the other materials, including the less reactive monomer.²⁰ This produces copolymers with properties similar to a semi-continuous process using a monomer mixture, but in a shorter reaction time.

In both batch and semi-batch emulsion polymerization, the transfer of monomers from the monomer droplets to the polymer particles is controlled by their solubility and diffusion in the water phase. This limits the range of monomers that may be used in emulsion reactions: Very hydrophobic monomers do not dissolve readily, and therefore do not incorporate well into the copolymer.

All the emulsion polymerization protocols described have advantages and disadvantages. The monomers used in this project were not extremely hydrophobic, so miniemulsion polymerization was not deemed necessary. Since ensuring a uniform distribution of monomers within the latex particles was critical to the success of the project however, semi-batch emulsion copolymerization was selected to synthesize the pyrene-labeled latex particles.

1.3 Methods to Probe IPD

1.3.1 Small-Angle Neutron Scattering (SANS)

Due to the lack of proper experimental methods, IPD was not studied until the late 1980's. Although interparticle diffusion was widely suspected to occur to yield latex films with good mechanical properties, electronic micrographs revealed that the honeycomb structure, typically observed for a film made of closely packed latex particles, was still present even after prolonged annealing times,

suggesting that IPD had not occurred. A more thorough investigation into the phenomenon was needed, for which SANS was employed.¹⁰

SANS measures the scattering of a neutron beam after it interacts with the nuclei of atoms. This experiment was used to characterize latex films where a fraction of the particles within the sample matrix were deuterated. These deuterated particles were mixed with protonated latex particles otherwise identical in size, polymer molecular weight distribution and chemical composition. Contrast was observed between the deuterated and protonated particles, since the scattering length for hydrogen and deuterium is significantly different. This difference in scattering power made it possible to measure the radius of gyration (R_g) of the latex particles, which is related to the radius of a solid sphere (r) through Equation 1-4.²²

$$R_g = \sqrt{\frac{3}{5}}r \quad (1-4)$$

Guinier's law was used to determine the radius of gyration from the scattering data, for which the scattered intensity is proportional to a form factor $P(q)$, whose expression for small scattering vectors

$q = 4\pi \sin \frac{\theta}{\lambda}$ is given as a function of R_g and q by Equation 1-5.²²

$$P(q) = 1 - \frac{1}{3}R_g^2 \times q^2 \quad (1-5)$$

Since IPD results in expansion of the deuterated latex particles, measuring the radius of gyration with respect to temperature and annealing time provides a measure of the extent of diffusion taking place in the latex film. However, a more quantitative measure of the IPD is obtained by determining the diffusion coefficient (D) of the polymer chains constituting the latex particles. In turn, the radius of gyration is related to the diffusion coefficient through Equation 1-6,¹⁰

$$R_g^2(r_0) = \frac{\int C(r,t)r^4 dr}{\int C(r,t)r^2 dr} \quad (1-6)$$

where $C(r,t)$ is the concentration of the deuterated monomer units diffusing into the protonated matrix and t is the diffusion time, as defined by Equation 1-7.

$$C(r,t) = \frac{C_0}{2} \left\{ \operatorname{erf}\left(\frac{R+r}{2\sqrt{Dt}}\right) + \operatorname{erf}\left(\frac{R-r}{2\sqrt{Dt}}\right) \right\} - \frac{C_0}{r} \sqrt{\frac{Dt}{\pi}} \left\{ \exp\left(-\frac{(R-r)^2}{4Dt}\right) - \exp\left(-\frac{(R+r)^2}{4Dt}\right) \right\} \quad (1-7)$$

$C(r,t)$ in Equation 1-7 is calculated with a D -value which is optimized by matching the ratio of the integrals in Equation 1-6 determined mathematically with the value of R_g^2 determined experimentally. While IPD in latex films can be characterized effectively by SANS, the procedure is limited to small latex particles with an upper diameter limit of 60 nm. Thus SANS would have little use for larger latex particles such as those characterized in this thesis, whose diameter was ca. 100 nm.

1.3.2 Förster Resonance Energy Transfer (FRET)

The upper limit of 60 nm for the diameter of latex particles studied by SANS led to a search for techniques to study IPD in films prepared from larger latex particles. A procedure based on FRET was proposed to achieve this task. In this procedure, some latex particles are labeled with an energy donor (D), and others are labeled with an energy acceptor (A). Mixing of the components in the two latex particles brings the energy donor near an energy acceptor, which allows the excess energy of the donor to be transferred to the acceptor via FRET. The FRET efficiency can be quantified and used to determine the extent of IPD in the latex film, which is related to the diffusion coefficient of the polymer chains in the film. Figure 1-4 illustrates how IPD leads to mixing of the donor- and acceptor-labeled chains during film formation.⁶

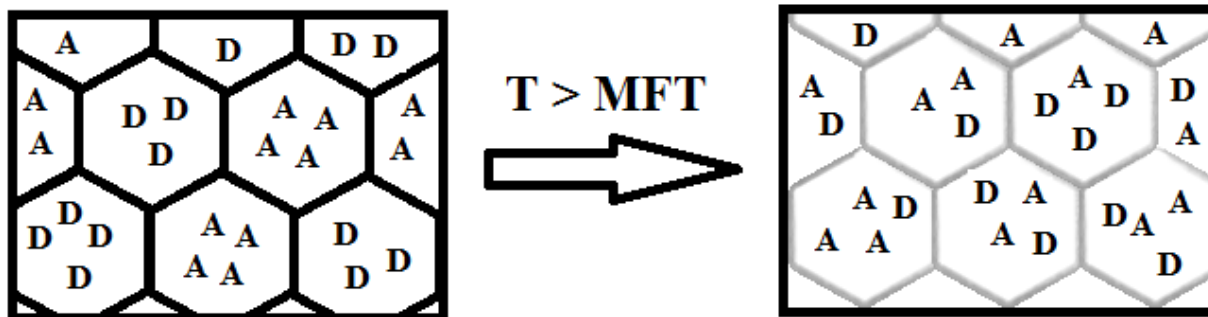


Figure 1-4: Diagram showing the mixing of the donor- and acceptor-labeled polymers before and after film formation.

By definition, FRET represents the radiationless transfer of excess energy from an excited fluorophore to a ground-state energy acceptor. In turn, fluorescence is the result of a photophysical process whereby the excitation of a fluorophore at a wavelength λ_{ex} results in the emission of a photon at a longer wavelength λ_{em} . The absorption of a photon at λ_{ex} results in the excitation of the fluorophore to one of the vibrational levels of its upper electronic states. Internal conversion relaxes the fluorophore to the lowest vibrational level of the S_1 electronic state. Relaxation from S_1 to one of the vibrational levels of the S_0 electronic state results in the emission of a fluorescence photon at wavelength λ_{em} . The entire process is depicted in the Jablonski diagram shown in Figure 1-5.

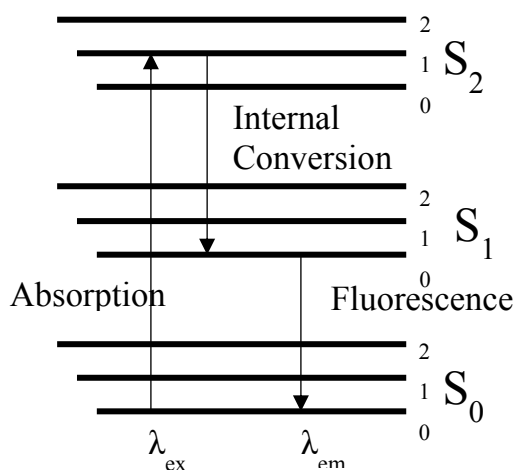


Figure 1-5: Jablonski diagram describing the fluorescence process.

A FRET study requires a donor and an acceptor molecule. When excited by light, the donor fluoresces with a lifetime τ_D . However if the excited donor happens to be nearby an acceptor molecule, the donor molecule may transfer its excess energy to the acceptor molecule, which becomes excited in the process and fluoresces with a lifetime τ_A . Efficient FRET occurs if there is sufficient overlap between the emission spectrum of the donor and the absorption spectrum of the acceptor. The fluorescence intensity of the donor in the absence (F_D) and the presence (F_{DA}) of an acceptor is measured using time-resolved fluorescence.²¹ The FRET efficiency (E_{ET}) between an excited donor and a ground-state acceptor depends on whether the distance separating the donor from the acceptor (R) is greater or smaller than the Förster radius (R_o). The magnitude of R_o can be determined experimentally for any donor/acceptor pair and typically ranges between 1 and 10 nm. The efficiency of FRET (E_{ET}) can be calculated using Equation 1-8, which in turn can be applied to determine the distance between a donor and an acceptor from E_{ET} .

$$E_{ET} = 1 - \frac{F_{DA}}{F_D} = \frac{R_o^6}{R_o^6 + R^6} \quad (1-8)$$

Before the particles coalesce, the donor and acceptor labels are confined within their respective latex particles and FRET only occurs across the particle boundaries. As the polymer chains diffuse, donor and acceptor molecules come within shorter distance and FRET takes place more efficiently based on Equation 1-8. Once a film composed of two individually labeled latex particles is prepared, the fluorescence decays for the donor are acquired and fitted with Equation 1-9. The first part of Equation 1-9 represents those donors that are close to an acceptor and are subject to FRET, while the second half of the equation represents those donors that are too far from an acceptor and emit with their own lifetime τ_D . Since the parameters B_1 and B_2 retrieved from the fit are proportional to the concentration of donors in the film that are or are not subject to FRET, respectively, they can be rearranged with Equation 1-10 to yield the uncorrected fraction of mixing

(f_m'). However because FRET can occur at the particle interface between the donor- and acceptor-labeled particles before any IPD has occurred, f_m' does not equal zero when film annealing starts. The non-zero value of f_m' is corrected using Equation 1-11 to calculate the true fraction of mixing (f_m), such that f_m equals zero before annealing has taken place.

$$I_D(t) = B_1 \exp\left(-\frac{t}{\tau_D} - 2\gamma\left(\frac{t}{\tau_D}\right)^{1/2}\right) + B_2 \left(\exp\left(-\frac{t}{\tau_D}\right)\right) \quad (1-9)$$

$$f_m' = \frac{B_1}{(B_1 + B_2)} \quad (1-10)$$

$$f_m(t) = \frac{f_m'(t) - f_m'(0)}{f_m'(\infty) - f_m'(0)} \quad (1-11)$$

A Fickian spherical diffusion model can be applied to obtain the diffusion coefficient using Equations 1-9 to 1-12. This is accomplished by equating Equations 1-11 and 1-12, where the concentration of donor-labeled polymer still present within the original boundaries of the latex particle is determined with Equation 1-7, where the only unknown is the diffusion coefficient D . The procedure involves adjusting D in Equation 1-7 until the calculated f_m value obtained in Equation 1-12 matches the f_m value obtained experimentally with Equation 1-11.

$$f_m(t) = 1 - \frac{\int_0^R C(r, Dt) \cdot 4\pi r^2 dr}{\frac{4}{3}\pi R^3 C_0} \quad (1-12)$$

The downside to this technique is that two types of labeled particles must be synthesized and all the particles must be fluorescently labeled, making it difficult to study a native latex prepared in another laboratory. As will become clear by reading this thesis, the procedure based on PEF relaxes these requirements.

1.3.3 Pyrene Excimer Fluorescence (PEF)

Pyrene is a widely used fluorophore, because of its good quantum yield and high molar extinction coefficient. This makes it possible to acquire noise-free fluorescence spectra at low pyrene concentrations. Pyrene can be excited in the UV region, around 344 nm, and fluoresces between 350 and 600 nm. An encounter between an excited and a ground-state pyrenyl moiety can result in pyrene excimer formation. The excimer fluorescence is broad, structureless and centered around 475 nm. If an excimer is not formed, pyrene emits with its monomer lifetime and the fluorescence spectrum exhibits 4 – 5 sharp peaks, depending on the solvent used. Figure 1-6 shows a fluorescence spectrum for pyrene-labeled poly(*n*-butyl methacrylate) (PBMA) acquired in THF. The spectrum has two dominant peaks at 375 nm for I₁ and 395 nm for I₄, the I₂ and I₃ peaks being much more suppressed at 383 and 387 nm, respectively. The excimer fluorescence centered at 475 nm is also clearly visible in the spectrum.

As can be seen from the kinetic scheme shown in Figure 1-6, pyrene excimer fluorescence (PEF) follows from the contact encounter between two pyrenyl groups, which depends on the local pyrene concentration, a higher concentration resulting in more encounters. Consequently, PEF is a measure of the local pyrene concentration and should be useful to study IPD taking place during latex film formation, in the same way that the FRET efficiency provided a measure of the local acceptor concentration surrounding the donors. The main difference between PEF observed in a solution as in Figure 1-6 versus a latex film is that the excimer is dynamic in solution, but static in the solid state, hence the dashed arrow representing dynamic encounters between an excited and a ground-state pyrene. As a matter of fact, excimer formation in the solid state results from the equilibrium between unassociated pyrenes that emit as monomer, and aggregated pyrenes that generate PEF. Contrary to PEF in solution, no diffusive encounters between pyrene labels can occur in the solid state over a time span of 1 μ s, when pyrene is excited.

A procedure was implemented whereby latex particles labeled with pyrene were mixed with an excess of non-labeled latex particles having the same diameter and polymer molecular weight distribution as the fluorescent latex particles. Upon annealing the film the pyrene-labeled chains diffused out of the latex, resulting in a decrease in the local pyrene concentration and a reduction in PEF. A schematic representation of the effect that IPD has on the distribution of the pyrene labels in the film is shown in Figure 1-7.

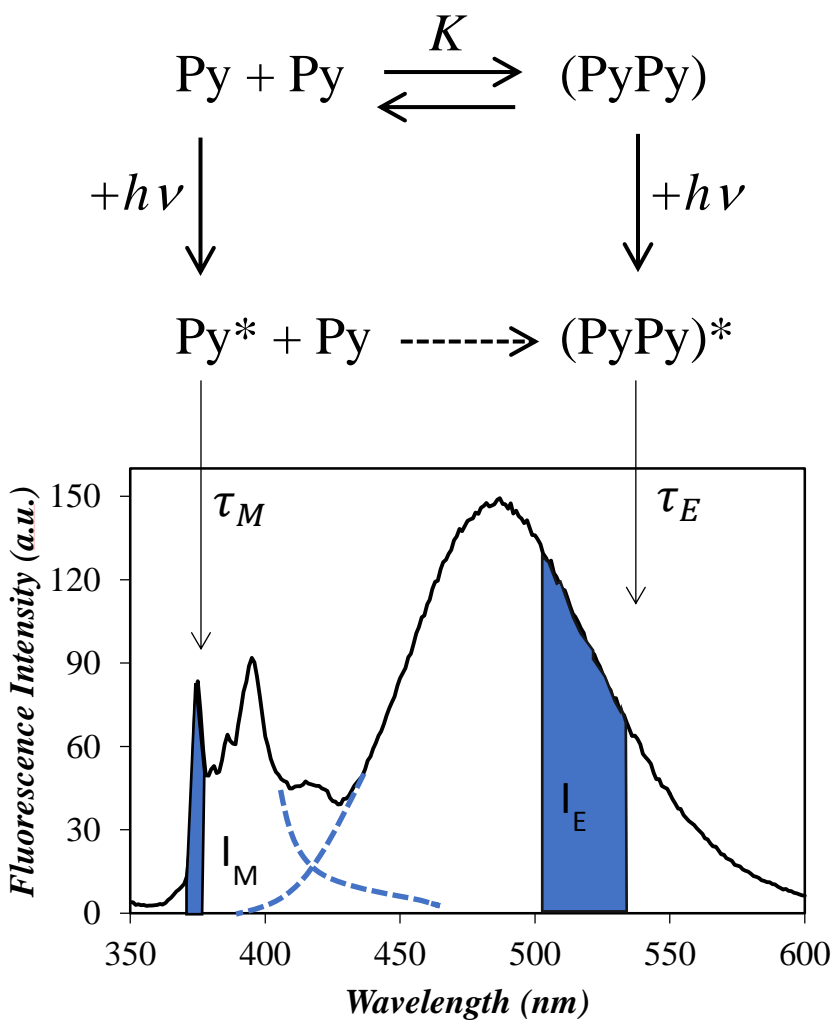


Figure 1-6: Top: Kinetic scheme representing pyrene excimer formation through encounters between an excited and a ground-state pyrene. Bottom: Resulting steady-state fluorescence spectrum.

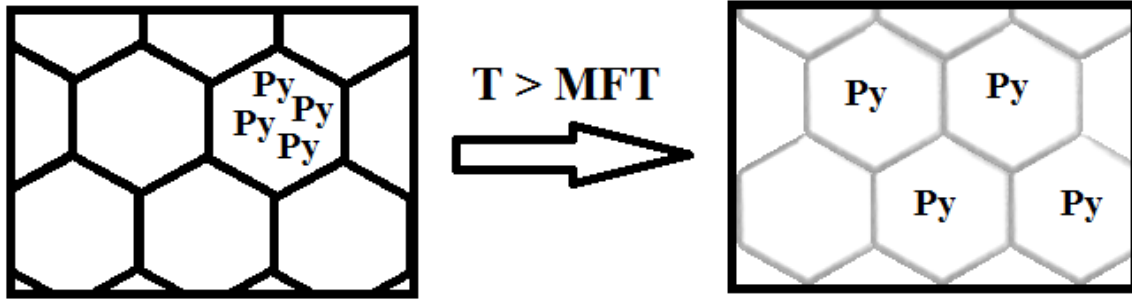


Figure 1-7. Change in distribution of pyrene labels in a latex film during film formation from (left) when the particles have deformed but no IPD has taken place to (right) a fully annealed film.

The magnitude of PEF was characterized as a function of annealing time by determining the ratio of fluorescence intensity for the excimer over that for the monomer, namely the I_E/I_M ratio, at different time intervals during film annealing. In turn, the I_E/I_M ratio could be employed to determine the fraction of mixing as shown in Equation 1-13. At this stage, the same procedure described for the FRET-based method (see Equations 1-9 to 1-12) was applied to determine the diffusion coefficient of the polymer chains in the latex film.

$$f_m(t) = \frac{\left(\frac{I_E}{I_M}\right)_t - \left(\frac{I_E}{I_M}\right)_0}{\left(\frac{I_E}{I_M}\right)_\infty - \left(\frac{I_E}{I_M}\right)_0} \quad (1-13)$$

Besides the fact that only one type of latex particle needs to be labeled, another advantage of the PEF-based method is the change in color emitted by the film as IPD takes place. Since the pyrene monomer and excimer emit purple and green fluorescence, respectively, changes in the relative concentrations of monomer and excimer during annealing result in changes in film color. Such changes have been observed as a function of film annealing, which indicates that these color changes

could be harnessed to monitor film annealing visually. In turn, this feature could provide an easier means to probe the extent of film formation.¹²

1.4 Thesis Outline

While an earlier study demonstrated the validity of the PEF-based procedure in terms of its ability to probe IPD during latex film formation, either quantitatively through the measure of the I_E/I_M ratio or qualitatively by visually monitoring color changes during film annealing, it was also recognized that the latex films generated very little PEF due to the low pyrene content of the pyrene-labeled latex particles. Indeed, only 1.9 mol% of the structural units constituting the poly(*n*-butyl methacrylate) component of the latex particles bore a pyrenyl group. This 1.9 mol% incorporation of pyrene-labeled monomers (PyLM) was the highest reached within a series of PyLMs that were prepared for the M.Sc. thesis of Remi Casier, where the pyrenyl group was linked to the methacrylate monomer via an oligo(ethylene glycol) (EG_{*n*}) spacer with a degree of polymerization (DP = *n*) equal to either 1, 2, 3, 9, or 71. Increasing *n* in the EG_{*n*} spacer was expected to enhance the water solubility of the corresponding PyLM. The PyLMs need to be sufficiently water-soluble to ensure their incorporation into the latex particles prepared by emulsion polymerization, since the monomers must diffuse through the aqueous phase from the monomer droplets to the polymer particles. The high hydrophobicity of pyrene would have prevented any incorporation of PyLM into latex particles if an EG_{*n*} spacer had not been added. Consequently, the level of pyrene incorporation into the latex was monitored as a function of the EG_{*n*} spacer length in the work of Casier.

When PyLMs with 1 or 2 ethylene glycol units were copolymerized with *n*-butyl methacrylate, latex particles containing, respectively, 0.9 and 1.3 mol% pyrene were obtained, which generated insufficient PEF to observe a clear decrease in the I_E/I_M ratio as a function of annealing time. PyEG₉MA and PyEG₇₁MA were also copolymerized but yielded crosslinked polymers. Since

crosslinking would prevent polymer diffusion, the latex particles prepared with the PyLMs having longer EG_n spacers were not used for the IPD studies. Consequently, only the latex particles labeled with 1.9 mol% of PyEG₃MA were employed to study IPD during latex film formation by PEF. However, even these fluorescent latex particles generated relatively little PEF and it was recognized that the PEF-based procedure would benefit greatly from the use of a pyrene-labeled latex generating more PEF through increased incorporation of the PyLM.

Thus the goal of this project was to optimize the design and the synthesis of the PyLMs, to enable their higher incorporation into latex particles and provide a stronger PEF signal. As will be discussed in Chapter 2, PyEG_nMA monomers with $n = 4, 5, 6.5,$ and 7.4 were synthesized in an attempt to generate monomers that would incorporate more easily into the copolymer, resulting in a stronger PEF signal. These monomers were characterized by ¹H NMR spectroscopy, gel permeation chromatography (GPC), UV-Vis absorption, and steady-state and time-resolved fluorescence spectroscopy. The PyLM with $n = 4$, and the corresponding latex particles were studied by M.Sc. student Xiaozhou Chang and were not considered in this work. The remaining PyLMs were copolymerized with *n*-butyl methacrylate and yielded crosslinked polymers initially. It was thus necessary to modify the emulsion polymerization procedure to prevent crosslinking. To this end, a chain transfer agent (CTA) was employed. By adding a CTA, chain transfer occurred predominantly through the weak chemical bond of the CTA instead of the polymer. The resulting polymers were characterized by differential scanning calorimetry (DSC), GPC, UV absorbance, dynamic light scattering (DLS), and by steady-state and time-resolved fluorescence, as discussed in Chapter 2.

The fluorescently labeled latex was mixed with an unlabeled latex of a polymer having a similar molecular weight. The I_E/I_M ratio of the film was monitored as a function of annealing time using steady-state fluorescence, as described in Chapter 4. Although addition of the CTA minimized crosslinking, aggregation of the PyLM into flower-like micelles in solution apparently also promoted

aggregation of the pyrene labels in the polymer, which resulted in unresolved issues in the film formation process. The materials obtained were thus unsuitable to monitor film formation on a quantitative basis. How these conclusions were reached is described in the following chapters.

Chapter 2

Monomer Synthesis

The procedure implemented in this thesis to probe interparticle diffusion by pyrene excimer fluorescence (PEF) required the preparation of fluorescent latex particles, constituted of chains labeled with the dye pyrene. This was achieved by copolymerizing the monomer of interest, *n*-butyl methacrylate, with a pyrene-labeled monomer (PyLM) by emulsion polymerization. As stated in the Introduction, emulsion polymerization requires that the monomers diffuse across the water phase from the monomer droplets to the polymer particles, where polymerization occurs. In turn, this requirement imposes that the PyLM reside in the water phase for some time, a condition that is complicated by the hydrophobicity of pyrene. This problem was addressed by introducing water-soluble motives in the PyLM to promote its water solubility. The different steps involved in the synthesis and characterization of the PyLMs are described hereafter.

2.1 Materials

Acetone (Sigma-Aldrich, 99.9%), ammonium persulfate (APS, Sigma-Aldrich, 98%), *n*-butyl methacrylate (BMA, Sigma-Aldrich, 99%), calcium hydride (CaH₂, Aldrich, 98%), 4-

dimethylaminopyridine (DMAP, Alfa Aesar, 99%), dioctyl sodium sulfosuccinate (AOT, Sigma-Aldrich, 98%), ethanol (Fisher Scientific, HPLC grade), ethyl acetate (Sigma-Aldrich, 99.7%), hexane (mixture of isomers, Sigma-Aldrich, 98.5%), methacrylic anhydride (Sigma-Aldrich, 94%), methanol (Sigma-Aldrich, 99.9%), nitromethane (Sigma-Aldrich, 99%), penta(ethylene glycol) (Sigma-Aldrich, 98%), phenylmagnesium chloride (Sigma-Aldrich, 2M in THF), silver (I) oxide (Sigma-Aldrich, 99%), sodium bicarbonate (BDH, 99.7%), tetrahydrofuran (THF, Sigma-Aldrich, 99%), tetrahydrofuran (distilled in glass, inhibitor-free, Caledon), *p*-toluenesulfonyl chloride (Sigma-Aldrich, 96%), triethylamine (Sigma-Aldrich, 99%), and tetra(ethylene glycol) (Sigma-Aldrich, 98%) were used as received.

Dichloromethane (DCM, Sigma-Aldrich, 99.8%) was freshly distilled prior to use. N,N-Dimethylformamide (DMF, Sigma-Aldrich, 99.8%) was distilled under reduced pressure on 4A molecular sieves immediately prior to use.

Ethylene oxide (Praxair) was purified by the following procedure. A glass manifold was mounted on a high vacuum line with a supply line to the ethylene oxide tank and an ampule containing CaH₂. The manifold was flame-dried twice below 0.1 mm Hg. The ampule containing CaH₂ was sealed after cooling and the system was purged with dry nitrogen. Phenylmagnesium chloride (2 M in THF) was added to the round-bottom flask and the THF was removed under vacuum. The round-bottom flask was then placed in an ice bath to transfer and condense the ethylene oxide, which was then stirred for 10 minutes before freezing in liquid nitrogen. Once the content was frozen, the manifold was evacuated. The freeze-pump-thaw cycle was repeated three times. In the final cycle, ethylene oxide was thawed and recondensed into the ampule containing CaH₂. CAUTION: Since ethylene oxide is highly toxic and volatile, extreme caution should be taken in handling that material in a well-ventilated fume hood.

Sodium hydride (Sigma-Aldrich, 60% dispersion in mineral oil) was washed twice with diethyl ether prior to use.

2.2 Instrumentation

¹H NMR: Samples were prepared in deuterated dimethyl sulfoxide (Sigma-Aldrich, 99.9% D) or deuterated chloroform (Sigma-Aldrich, 99.8% D) and measured on a 300 MHz Bruker spectrometer.

Dynamic Light Scattering (DLS): Samples were prepared by adding one drop of latex solution to a 2 mL vial with deionized water. The measurements were carried out on a Brookhaven BI-200SM instrument. A BI-9000AT digital autocorrelator was used to analyze the data and obtain information on the particle size and dispersity.

Gel Permeation Chromatography (GPC): Samples were prepared at a concentration of 1 mg/mL in THF and filtered through a 0.2 μm Teflon filter. A Viscotek VE 2001 GPC was used with a TDA 305 triple detector array and a UV detector model 2600 to obtain the differential refractive index (DRI), right-angle light scattering (RALS), low-angle light scattering (LALS) and UV absorption signals with respect to the elution volume. A series of 10^4 - 10^5 Å PolyAnalytik SupeRes mixed bed columns were used to separate the analytes.

Steady-State Fluorescence: Samples were prepared both in the solid state and in solution. Solid state samples were prepared in a 1 cm \times 1 cm quartz tube fitted with a rubber septum. A front-face geometry was used for solid-state samples. Samples in solution were prepared in fluorescence-grade THF with an absorbance of less than 0.12 at 344 nm and degassed gently for one hour in a 1 cm \times 1 cm quartz cell. Both sets of samples were excited at 344 nm and scanned from 350 to 600 nm on a Photon Technology International instrument.

Time-Resolved Fluorescence: Fluorescence decays were acquired for solutions of PyLMs and their polymers which were prepared in the same manner as for the steady-state fluorescence experiments. The solutions were excited at 344 nm and the emissions of the monomer and excimer were acquired at 375 and 510 nm, respectively. An IBH time-correlated single photon counting (TC-SPC) fluorometer was used to obtain the decays. Optimization programs developed in-house were used to fit the decays with sums of exponentials.

UV-Visible Absorbance: Samples were prepared in a quartz cell with a 1 cm path length using fluorescence-grade THF. A Cary 100 Bio UV-Visible spectrophotometer was used to obtain the absorption spectra.

2.3 Synthesis of the PyLMs

2.3.1 Synthesis of Ethoxylated 1-Pyrenemethanol (PyEG_nOH)

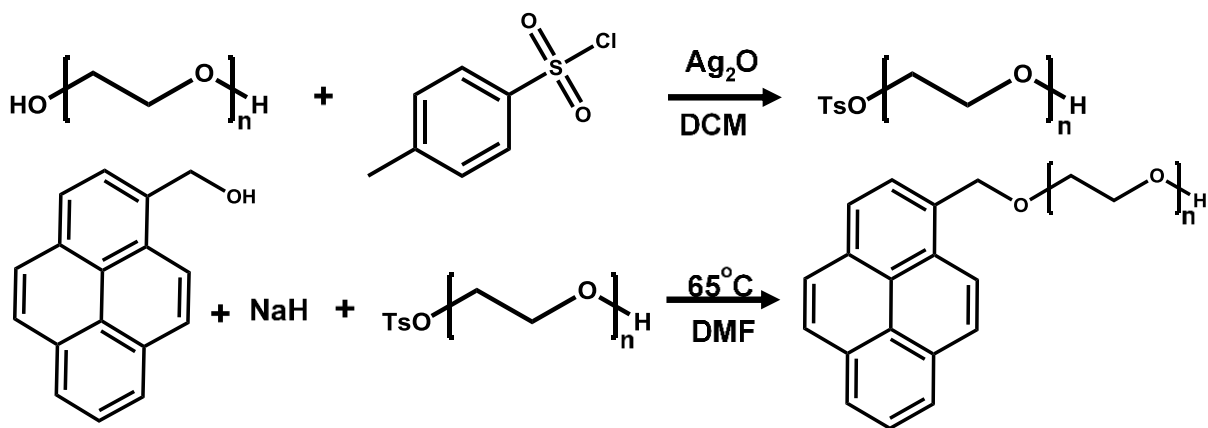
The preparation of the PyLMs began with the addition of oligo(ethylene oxide) to 1-pyrenemethanol (PyMeOH) to yield PyEG_nOH (where n represents the number of ethylene oxide units). This modification was achieved by either coupling an oligo(ethylene glycol) segment with PyMeOH, or anionically polymerizing ethylene oxide from sodium 1-pyrenemethoxide. The first approach was best for short spacers, up to penta(ethylene glycol) ($n = 5$), mostly due to the high cost of the longer oligo(ethylene glycol)s. Anionic polymerization was better suited for longer oligo(ethylene glycol) spacers.

2.3.1.1 Coupling of Oligo(Ethylene Glycol) Segments with 1-Pyrenemethanol

The preparation of PyEG₄OH according to Scheme 1 is described in detail hereafter. The oligo(ethylene glycol) was first tosylated. In a flame-dried round-bottom flask, tetra(ethylene glycol) (2.00 g, 8.39 mmol) and silver oxide (2.92 g, 12.59 mmol) were dissolved in distilled dichloromethane (DCM; 30 mL) under nitrogen. The solution was stirred for 30 minutes and placed in an ice bath. Tosyl chloride (1.76 g, 9.23 mmol) and potassium iodide (0.28 g, 1.68 mmol) were added to the flask and the mixture was stirred for 15 minutes. The mixture was then filtered over a Celite bed and the solvent was evaporated. The monotosylated product was separated from the doubly tosylated product by flash chromatography on silica gel with ethyl acetate as eluent. The resulting monotosylated tetra(ethylene glycol) was a clear, viscous liquid obtained in 82% yield.

The monotosylated tetra(ethylene glycol) was then coupled with PyMeOH. Sodium hydride (0.59 g, 24.6 mmol) was added to a flame-dried round-bottom flask, followed by PyMeOH (7.15 g, 30.8 mmol) and DMF under nitrogen, before the solution was stirred for one hour. Monotosylated tetra(ethylene glycol) (4.00 g, 10.3 mmol) was added and the flask was kept in a 65 °C oil bath overnight. After the reaction was complete, three liquid-liquid extractions were performed with 20 mL water and 20 mL DCM. The organic phase was evaporated and dried under vacuum overnight. The product was purified by flash chromatography over silica gel with ethyl acetate as eluent. The resulting ethoxylated PyMeOH (PyEG₄OH) was a viscous yellow liquid obtained in 40% yield. The chemical composition of PyEG₄OH was verified by ¹H NMR analysis, and its photophysical properties were characterized by steady-state and time-resolved fluorescence.

The procedure described in Scheme 2-1 was modified from a method proposed by Casier.¹² The original method, using 1-bromomethylpyrene as a starting material, yielded impure PyEG_nOH with complex fluorescence decays, contrary to what was reported in the thesis of Casier.



Scheme 2-1: Synthesis of PyEG_nOH by coupling of oligo(ethylene glycol) with PyMeOH.

Consequently, that procedure was not pursued further.

2.3.1.2 Synthesis of PyEG_nOH by Anionic Polymerization

The reaction for the anionic ethoxylation of PyMeOH is described in Scheme 2-2. 1-Pyrenemethanol was purified by recrystallization in ethanol. The vacuum manifold (Figure 2-1) was fitted with one ampule containing purified ethylene oxide and one clean, empty ampule on outlets A and B. The empty ampule and the manifold were evacuated and flamed to remove adsorbed moisture. The desired amount of ethylene oxide (ca. 1.1 mL) was then recondensed to the tared empty ampule by warming the ampule containing the ethylene oxide to room temperature and cooling the empty ampule in liquid nitrogen.

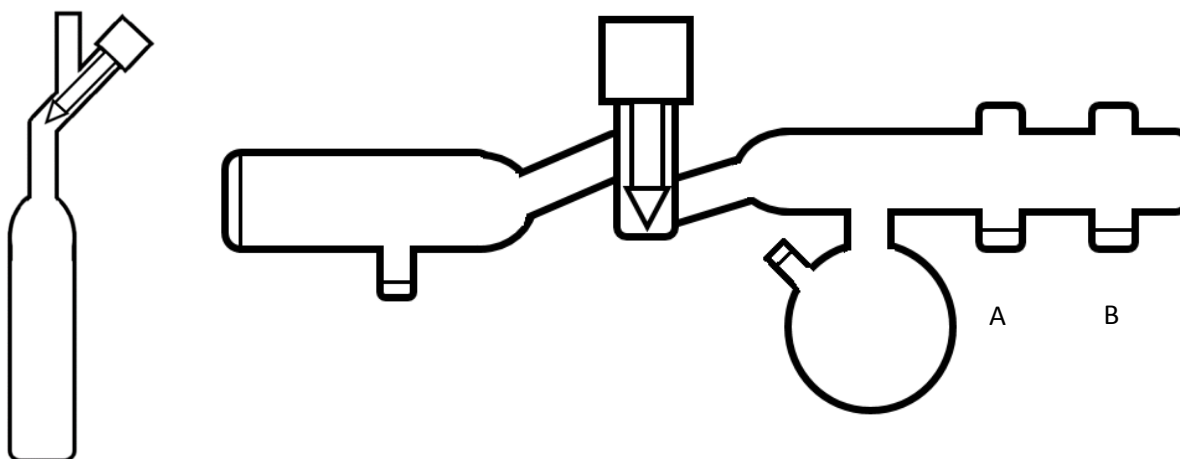
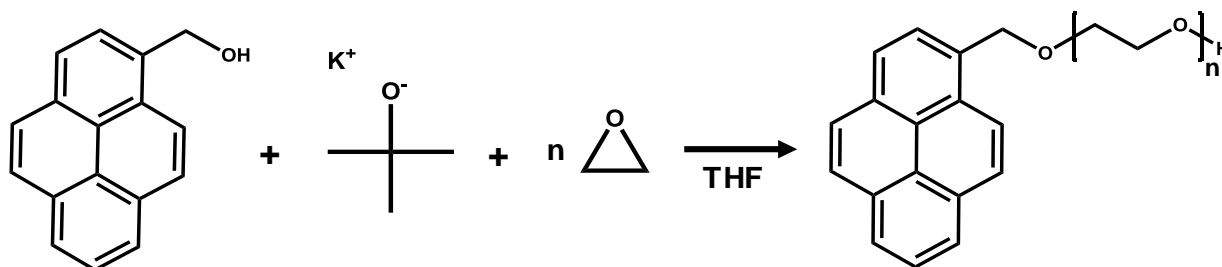


Figure 2-1: Diagram of an ampule (left) and vacuum line manifold (right).

The manifold was filled with dry nitrogen, the ampule was sealed and removed for weighing to obtain the exact mass of ethylene oxide transferred (1.19 g, 27.0 mmol). 1-Pyrenemethanol (1.05 g, 4.52 mmol, for a target $M_n = 496$ g/mol) was then loaded into the second ampule on the manifold, and potassium *tert*-butoxide (0.50 g, 4.45 mmol) was loaded into the same ampule inside a glove box. The ampule was then mounted again on the manifold and evacuated. Distilled THF (ca. 25 mL) was condensed into the second ampule under vacuum. The solution was stirred for one hour to allow

the deprotonation of 1-pyrenemethanol before it was frozen in liquid nitrogen, while the ethylene oxide ampule was allowed to warm to room temperature to transfer the monomer to the second ampule, which was then thawed and filled with nitrogen. After stirring for 10 minutes, the sealed ampule was removed and allowed to react for 96 hours at room temperature inside the fume hood. The polymerization was terminated with several drops of water. The solvent was removed under vacuum and purified by column chromatography over alumina using a 2 : 1 ethyl acetate : hexane mixture as eluent. The product could be clearly identified from its green fluorescence. It eluted as the second to last band, exhibiting green fluorescence. The product was recovered and the solvent was removed on a rotary evaporator. PyEG_nOH was a yellow oil obtained in 70% yield. The chemical composition of PyEG_nOH was confirmed by ¹H NMR analysis and its photophysical properties were characterized by steady-state and time-resolved fluorescence.

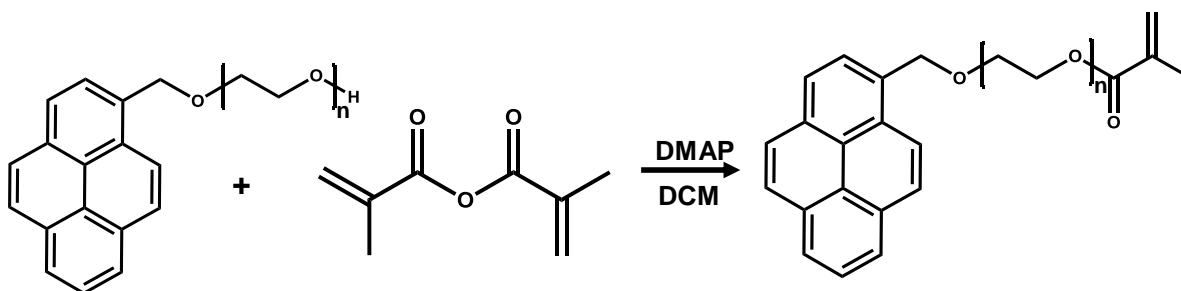


Scheme 2-2: Synthesis of PyEG_nOH by anionic polymerization.

2.3.2 Methacrylation of Ethoxylated 1-Pyrenemethanol

The PyEG_nOH derivatives were further reacted with methacrylic anhydride to obtain the corresponding PyLM as described in Scheme 2-3. The procedure used for PyEG₅OH is described in detail. PyEG₅OH (0.3 g, 0.73 mmol) and 4-dimethylaminopyridine (DMAP, 9.0 mg, 0.073 mmol) were dissolved in dry dichloromethane (10 mL) under nitrogen in an ice bath. Methacrylic anhydride (0.166 mL, 1.1 mmol) was added and the solution was stirred in an ice bath for 30 minutes before being allowed to warm to room temperature and stirred for 16 hours longer in the dark. A saturated

aqueous solution of sodium bicarbonate (15 mL) was then added to the solution which was stirred vigorously for 30 minutes before it was transferred to a separatory funnel and washed twice with saturated sodium bicarbonate solution (2×15 mL), and once with deionized water (15 mL). The solvent was removed and the product was purified by silica gel column chromatography using acetone with 0.1 vol% trimethylamine as eluent. The product in the second to last band, that exhibited green fluorescence, was collected and the solvent was removed under vacuum. The PyLM, obtained in a 70% yield, was a yellow viscous liquid. ^1H NMR spectroscopy was used to confirm the chemical composition of the PyLM, and its photophysical properties were characterized by steady-state and time-resolved fluorescence.



Scheme 2-3: Reaction of PyEG_nOH with methacrylic anhydride.

2.4 Characterization of the PyLMs

The primary techniques used to characterize the PyLMs were ^1H NMR to determine their chemical composition, steady-state and time-resolved fluorescence to establish their photophysical properties, and gel permeation chromatography (GPC) to confirm the oligomeric nature of the PyLMs.

The ^1H NMR spectra for a PyEG_{7,4}OH sample and its PyLM were acquired in CDCl_3 and are shown in Figure 2-2. The spectra were analyzed as follows: The integration value for the methylene protons of PyMeOH was compared with that for the ethylene oxide protons to determine the number-average degree of polymerization (DP_n) of the PyLMs synthesized by the anionic polymerization method. This was not necessary for the PyLMs synthesized via coupling, as the EG_n spacer would

have a well-defined DP. Based on this analysis, the first and second PyEG_nOH compounds obtained by anionic polymerization had DP_n of 7.4 and 6.5, as compared to target values of 8 and 7.4, respectively. Similar ¹H NMR spectra were obtained for the other PyEG_nOH samples and their corresponding PyLMs, the main difference being the relative magnitude of the peak at 3.7 ppm reflecting the ethoxylation level of these pyrene derivatives.

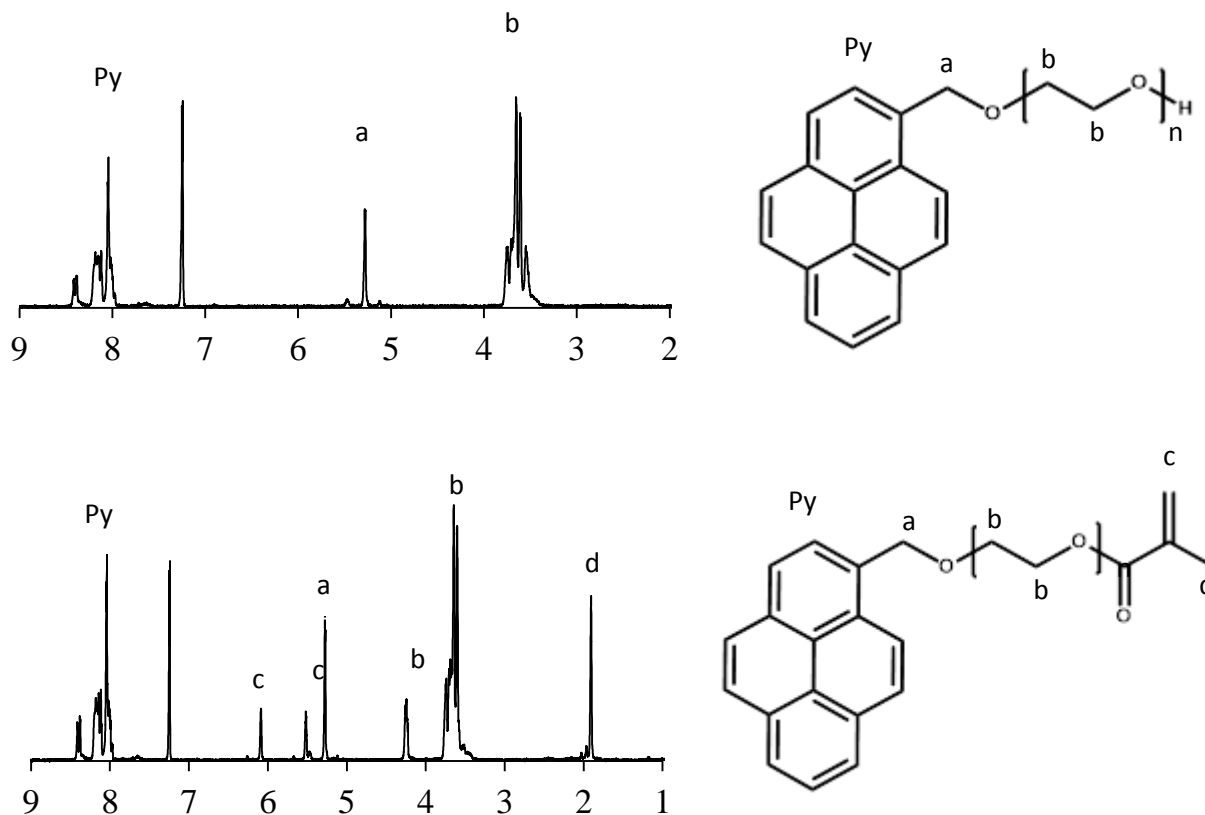


Figure 2-2: 300 MHz ¹H NMR spectra in CDCl₃ for PyEG_{7.4}OH and the corresponding PyLM in CDCl₃. Top: δ 8.0-8.4 (m, 9 H), 5.3 (s, 2 H), 3.4- 3.9 (m, 29.6 H). Bottom: δ 8.0-8.4 (m, 9 H), 6.1 (s, 1H) 5.5 (s, 1 H), 4.2 (m, 2 H), 5.3 (s, 2 H), 3.4- 3.9 (m, 27.6 H), 1.9 (s, 3 H). Residual solvent peaks are present at δ 7.2 ppm for CHCl₃.

Fluorescence is notoriously sensitive to impurities, and the spectral quality of the pyrene derivatives prepared in this thesis was assessed by conducting steady-state and time-resolved

fluorescence experiments. Solutions of the PyEG_nOH and PyLMs were prepared in THF with an absorption of 0.1 at 344 nm, where the pyrene derivatives absorbed. Oxygen present in the solutions was outgassed by gently bubbling nitrogen for 30 minutes. The resulting steady-state fluorescence spectra displayed the four peaks characteristic for an excited pyrene monomer at 375, 380, 390, and 395 nm. The time-resolved fluorescence decays for PyEG_{7.4}OH and PyEG_{7.4}MA could be well-fitted with a sum of two exponentials with decay times of 280 and 270 ns, the longest decay time having a 93% pre-exponential weight. These fluorescence spectra and decays are shown in Figure 2-4. The lifetimes of 280 and 270 ns are typical for ethoxylated PyMeOH derivatives. The shorter component of the decay is attributed to degraded pyrene species that could not be separated from the product.

Finally, gel permeation chromatography (GPC) analysis was used to determine the molecular weight distribution (MWD) of the PyLMs, displayed in Figure 2-3. This was particularly important for the monomers synthesized by anionic polymerization, since this method would result in a distribution of oligo(ethylene glycol) chain length for the PyLMs. Figure 2-3 shows the DRI trace of PyEG_{7.4}MA and the starting material, 1-pyrenemethanol. The single peak indicates that the product is free of impurities, including the starting material. The PyEG_{7.4}MA peak is broader than the PyMeOH peak, however the light scattered by the oligomers was not strong enough to yield reliable absolute molecular weight information or PDI.

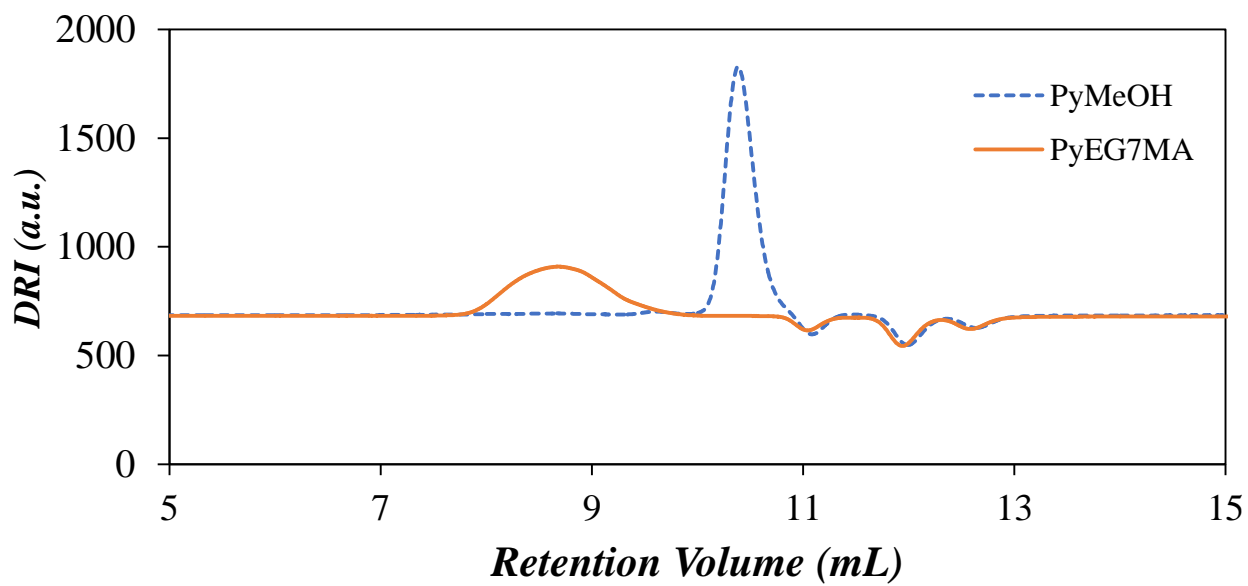


Figure 2-3: DRI traces for PyEG_{7.4}MA and PyMeOH.

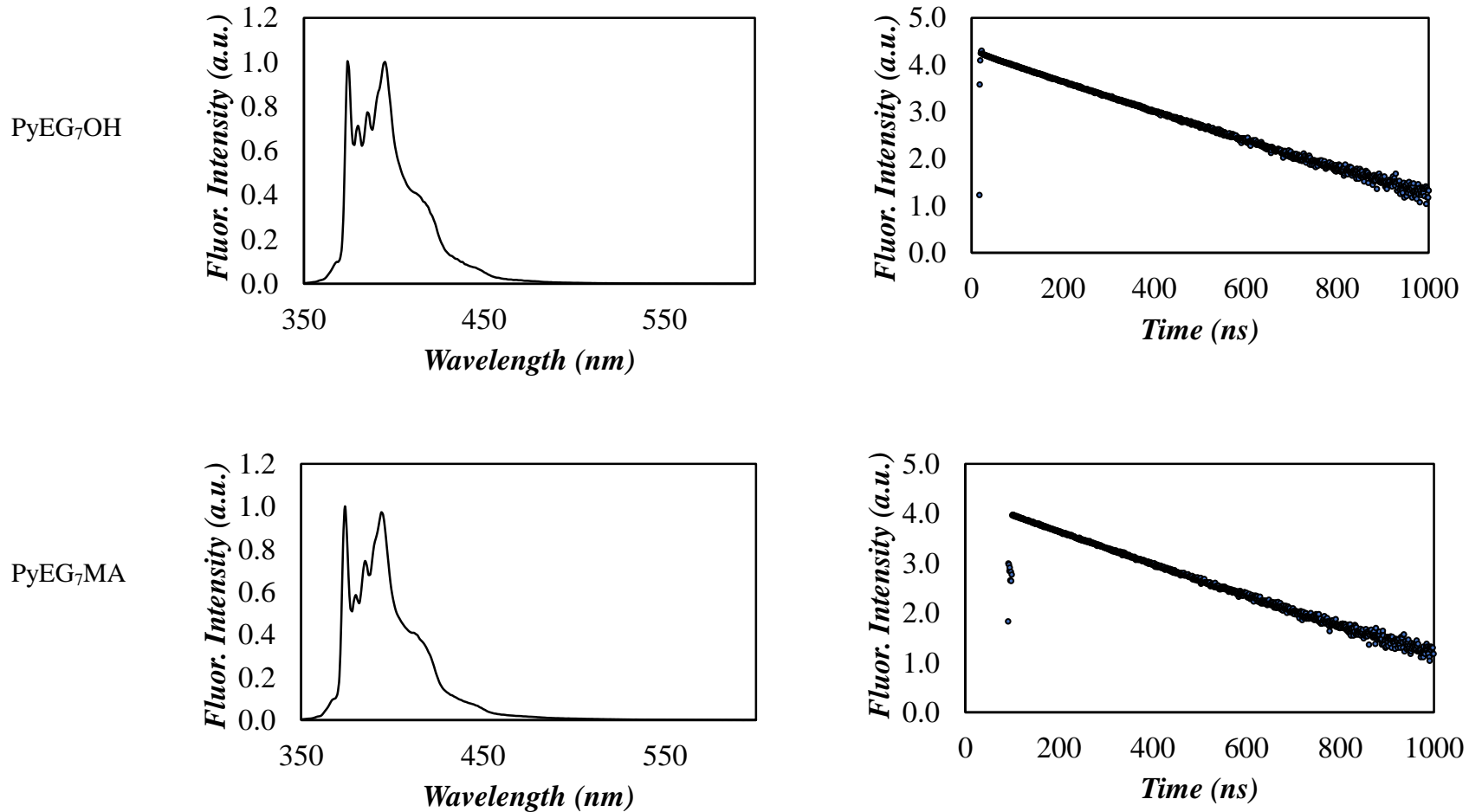


Figure 2-4: Steady-state fluorescence spectra (left) and time-resolved fluorescence decays (right) of ethoxylated 1-pyrenemethanol ($n = 7.4$) (top) with $\chi^2 = 1.00$, and the corresponding PyLM (bottom) with $\chi^2 = 1.10$

2.5 Aggregation of PyLM in Aqueous Solution

PyLMs with longer linkers ($n = 6.5$ and $n = 7.4$) appeared to form dispersions in water at the concentration used in the emulsion polymerization process. This is illustrated in Figure 2-5.

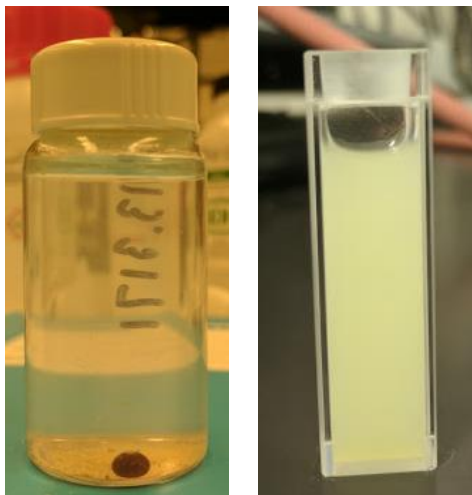


Figure 2-5: Left – Aqueous solution of PyEG₄MA, showing a single hydrophobic bead at the bottom of the vial. Right – Aqueous dispersion of PyEG_{7.4}MA at the same concentration.

The dispersion observed for the PyEG_{7.4}MA monomer in water suggested that it formed aggregates, probably micelles, with the hydrophobic pyrene and methacrylate groups forming the hydrophobic interior of the micelles stabilized by a corona made of hydrophilic oligo(ethylene oxide). The PyEG_{7.4}MA dispersions were further studied by time-resolved fluorescence. The PyLM was expected to be fully soluble in THF, where excimer formation would occur by diffusive encounters between an excited and a ground-state pyrene, which should result in a rise time in the excimer decay. On the other hand, micellization of the PyLM would result in the formation of pyrene aggregates in the micellar core, where excimer formation between two pyrene moieties would occur quasi-instantaneously and little to no rise time should be seen in the excimer decay. The excimer

fluorescence decays for a 5 mM PyEG_{7.4}MA solution in THF and water were compared in Figure 2-6.

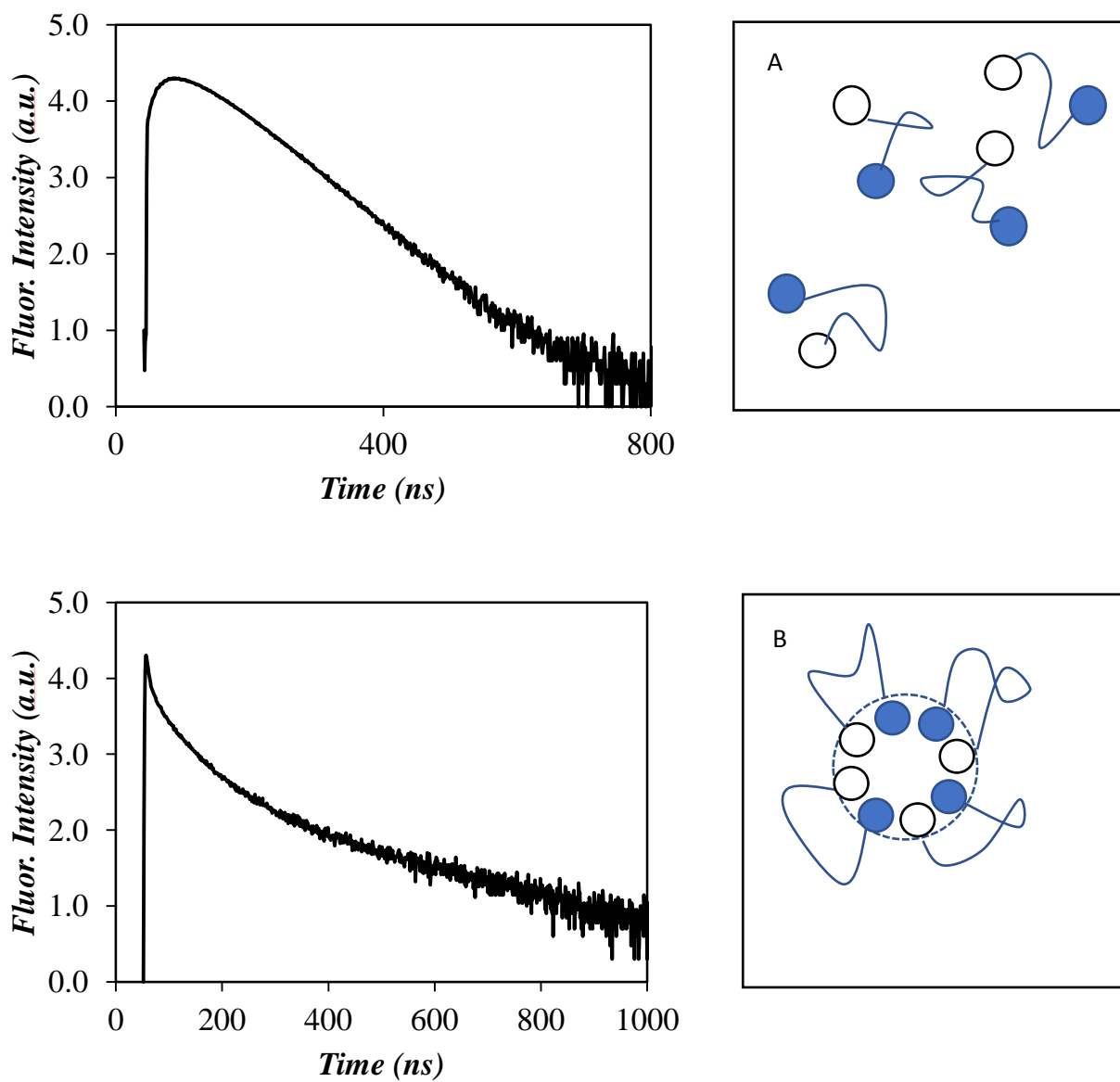


Figure 2-6: Time-resolved excimer fluorescence decays for 5 mM PyEG_{7.4}MA in A) THF and B)

water; $\lambda_{\text{exc}} = 344 \text{ nm}$, $\lambda_{\text{em}} = 510 \text{ nm}$.

The absence of a rise time in the excimer fluorescence decay of PyEG_{7.4}MA in Figure 2-6B is a clear indication that excimer emission occurs instantaneously by direct excitation of the pyrene aggregates. In turn, the existence of pyrene aggregates in the aqueous solution demonstrates that PyEG_{7.4}MA is not homogeneously solubilized in water and rather forms aggregates similar to micelles. Since initiation takes place in the aqueous phase for emulsion polymerization, the encounter of a growing oligomer with a PyEG_{7.4}MA micelle could result in the blocky incorporation of PyEG_{7.4}MA monomers, which would be sufficiently water-soluble to reside at the surface of the latex particles. This might result in a non-homogeneous distribution of the pyrene labels in the latex particles, complicating the analysis of the fluorescence data to characterize IPD occurring during latex film formation.

2.5 Summary

PyLMs with linkers of 4, 6.5, and 7.4 ethylene oxide units were synthesized. The analysis of the PyEG₄MA copolymer was conducted by Master's student Xiaozhou Chang. The remainder of this thesis will focus on the analysis of the copolymers using PyEG_{*n*}MA monomers with *n* equal to 6.5 and 7.4. All the monomers were shown to have good purity via ¹H NMR spectroscopy and steady-state and time-resolved fluorescence analysis. Aggregation of the PyLM in solution was observed and studied by time-resolved fluorescence. As a semi-batch procedure will be used to synthesize the particles, the observed micellization is not expected to affect the emulsion polymerization process dramatically.

Chapter 3

Particle Synthesis

Once the PyLM was synthesized as described in Chapter 2, a semi-batch emulsion polymerization procedure was applied to prepare the latex particles. To increase the incorporation of the PyLM into the copolymer, a water-soluble EG_n segment was introduced in the PyLM to promote its diffusion through the water phase in the emulsion polymerization. However, the potential for crosslinking in the polymer also increased for increasing degrees of polymerization of the EG_n moiety. A chain transfer agent (CTA) was employed to mitigate this problem. The occurrence of aggregation observed for the longer EG_n linkers, described in Section 2.5, was monitored to relate it to potential irregularities in the polymerization process. The steps involved in the synthesis and the

characterization of the latex particles, and the properties of the resulting polymers are described hereafter.

3.1 Synthesis of Latex Particles

Fluorescently labeled and unlabeled latex particles needed to be synthesized. The synthesis of the unlabeled latex will be described first. A 125 mL three-neck reactor flask (Figure 3-1) was fitted with a mechanical stirrer, a condenser and a rubber septum. The reactor was placed in an 80 °C oil bath. Deionized water (63 mL) and sodium docusate salt (AOT) (57 mg, 0.13 mmol) were added to the reactor and stirred while the system was purged with nitrogen for a minimum of 30 minutes. Ammonium persulfate (4 mg, 0.017 mmol) was then added. The needle used to purge the reactor with nitrogen was connected with a syringe containing a pre-emulsified solution of *n*-butyl methacrylate (2.0 g, 14.1 mmol), AOT (0.019 g, 0.043 mmol), dodecanethiol (0.72 mg, 0.0036 mmol) and deionized water (1 mL). Dodecanethiol was used as a chain-transfer agent to prevent crosslinking. The solution was transferred through a needle to the reactor over 3 hours via a syringe pump. Upon complete transfer of the syringe content to the reactor, stirring was stopped and the reactor was removed from the oil bath.

The same procedure was employed for the labeled latex, the PyEG_{7,4}MA monomer (0.42 g, 0.66 mmol) being added to the pre-emulsified solution to be injected into the reactor.

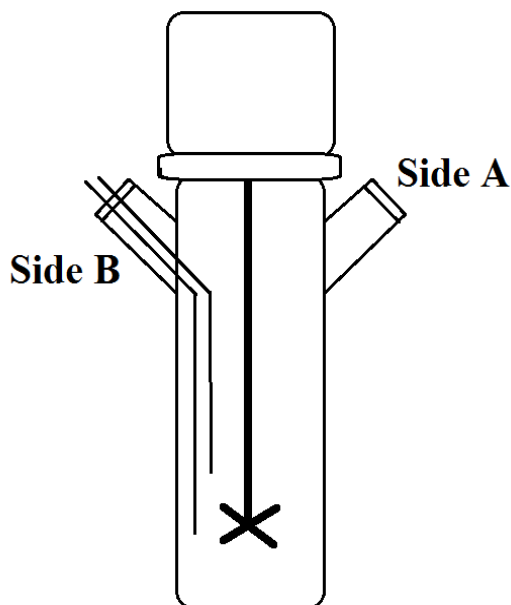


Figure 3-1: Three-neck reaction vessel used for emulsion polymerization. A condenser was fitted on Side A of the reactor and a rubber septum on Side B.

The latex dispersions were placed in a dialysis tube with a 50 kg/mol cutoff and dialyzed against a mixture of 80% water, 20% ethanol, and 5 mmol AOT for two weeks with gentle stirring and daily changes of the dialysate to remove unreacted monomer, initiator, and chain transfer agent. A sample of the polymers constituting the latex particles was isolated by precipitation. To this end, an aliquot was removed from the latex dispersion and freeze-dried. The freeze-dried dispersion was dissolved in a minimal amount of THF and methanol was added quickly to precipitate the polymer. The precipitate was removed from the solution and re-precipitated from THF thrice.

3.1.1 Addition of Dodecanethiol

Crosslinking was observed by Casier when conducting emulsion polymerization with PyEG_nMA monomers prepared with long oligo(ethylene oxide) segments ($n = 9$ and 71). The polymerization of PyEG₄MA was carried out without the addition of a chain transfer agent (CTA), but for longer linkers with $n \geq 5$, a CTA needed to be used to prevent crosslinking. Crosslinking is undesirable in film formation, as the polymer chains would be constrained and not be able to reptate freely across the particle boundary. A CTA also reduces the molecular weight of the polymer. Consequently, a balance between the initiator and CTA concentrations had to be found.

The Mayo equation (Equation 3-1) can be used to estimate the degree of polymerization (and molecular weight) of a polymer in the presence of a chain transfer agent.

$$\frac{1}{DP_n} = \frac{1}{DP_0} + C_s \frac{[CTA]}{[Monomer]} \quad (3-1)$$

Previous studies in the Winnik laboratory, where FRET was applied to study film formation for PBMA latex, used dodecanethiol as a chain transfer agent. Since this approach was shown to work, this CTA was selected for this study as well. C_s was unknown for the PyLM-BMA copolymers. As a result, 10 mg (0.05 mmol) of CTA per g (10 mg/g) of monomer were initially used, as compared to 5.5 mg (0.024 mmol) of initiator. The concentrations were ultimately adjusted to 3.5 mg of initiator and 0.3 mg/g CTA to yield a suitable molecular weight. The GPC curves are shown in Figure 3-2. Plotting of $1/M_n$ as a function of the [CTA] as suggested by Equation 3-1 was not attempted, as the initiator concentration was also varied.

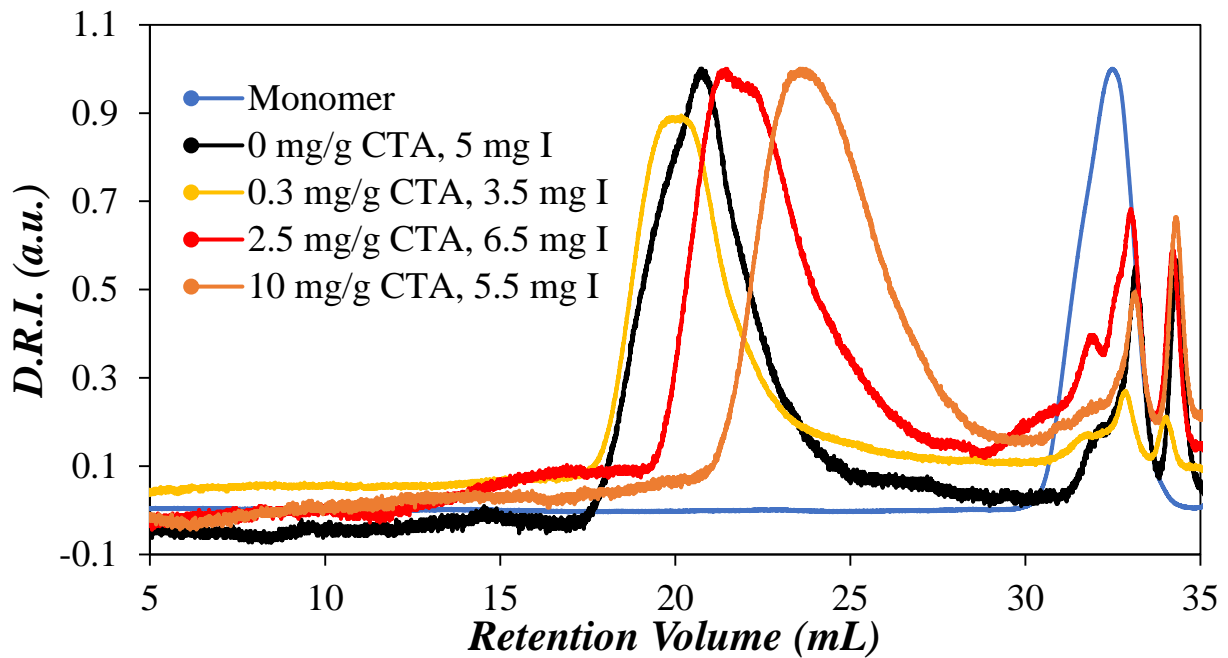


Figure 3-2: DRI GPC traces for copolymers synthesized at different CTA concentrations. Blue: Monomer, Black: [CTA] = 0 mg/g, [I] = 5 mg, Yellow: [CTA] = 0.3 mg/g, [I] = 3.5 mg, Red: [CTA] = 2.5 mg/g, [I] = 6.5 mg, Orange: [CTA] = 10 mg/g, [I] = 5.5 mg. 5% PyEG_{7,4}MA was used in all

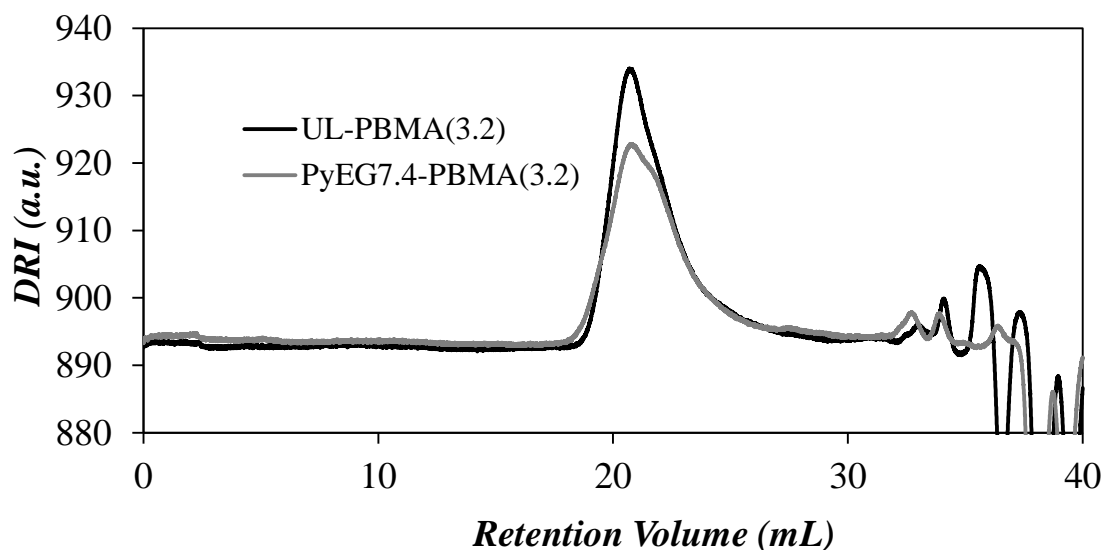
syntheses except for the 0 mg/g trial where 2% PyLM was used to minimize crosslinking as a molecular weight baseline.

3.2 Characterization of the Latex Particles

The characterization of the latex particles involved dynamic light scattering (DLS) to measure their hydrodynamic diameter (D_h) and a combination of GPC, differential scanning calorimetry (DSC), UV-Vis, and fluorescence measurements to determine the molecular weight distribution (MWD), the glass transition temperature (T_g), the pyrene content, and the extent of excimer emission for their constituting polymers, respectively. Table 3-1 summarizes the properties of the latex particles.

GPC was used to determine the MWD of the homo- and copolymers, since the polymers in the labeled and unlabeled latex particles should have similar MWDs. The PDI for polymers produced by emulsion polymerization is typically expected to be in the 2-3 range. The samples for GPC analysis were prepared by dissolving the precipitated polymer samples in THF at a concentration of 1 mg/mL. The resulting solution was filtered through a 0.2 μm Teflon filter and injected into the GPC for analysis. The labeled and unlabeled latex particles were constituted of polymers having M_n values of 230 and 260 kg/mol, with PDIs of 2.5 and 1.7, respectively. The overlaid GPC traces are shown in Figure 3-3.

To alleviate the concern that the properties of the native latex might change if a high percentage of PyLM was incorporated into the copolymer, particularly for PyLMs prepared with long EG_n linkers, the T_g of the labeled and unlabeled polymers was measured by DSC. The precipitated



polymer (10 mg) was placed in an aluminum pan and the heat flow was measured against an empty pan. The T_g of the unlabeled polymer was compared to the T_g of native poly(*n*-butyl methacrylate) (PBMA), known to range between 20 and 25 °C.²⁷ The DSC profile obtained for the PyEG_{7.4}-PBMA(3.2) sample is shown in Figure 3-4. It displays a transition corresponding to $T_g = 20$ °C, as expected for PBMA.

Figure 3-3: GPC traces for the unlabeled *n*-butyl methacrylate homopolymer and PyEG_{7.4}-PBMA(3.2).

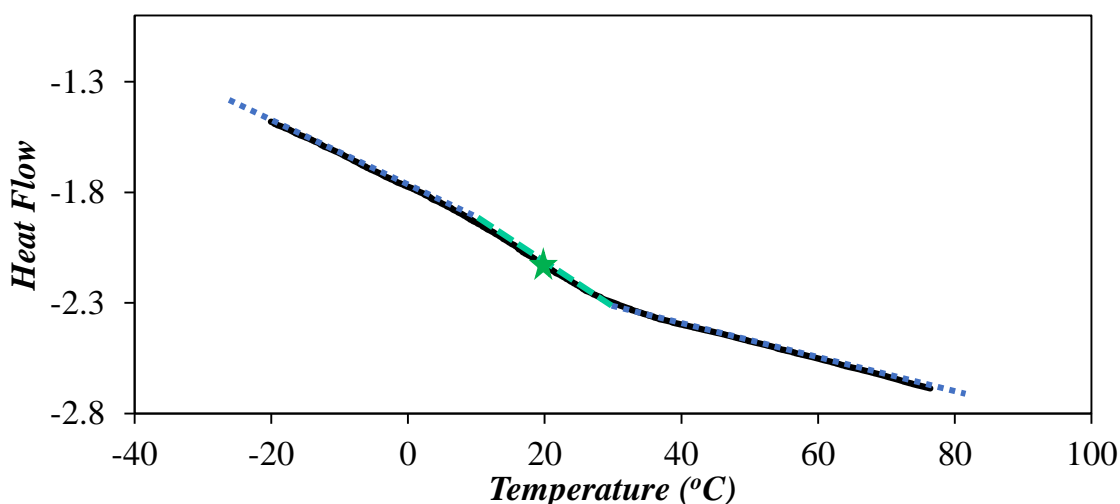


Figure 3-4: DSC profile for PyEG_{7.4}-PBMA(3.2) showing $T_g = 20$ °C.

Besides a similar MWD desired for the labeled and unlabeled polymers constituting the respective latex particles, the particles should also have a similar diameter. DLS was used to measure the hydrodynamic diameter of the latex particles, which are listed in Table 3-1.

The PDI values from DLS are different from the PDI obtained from GPC, in that 0 indicates a monodisperse size distribution. The PDI from DLS data is calculated using Equation 3-2.

$$PDI = \left(\frac{\sigma}{d} \right)^2 \quad (3-2)$$

In this equation, σ is the standard deviation and d is the mean diameter. Adding one to the PDI obtained by DLS would yield the PDI obtained from GPC, which is the ratio of the weight-average and number-average molecular weights. UV-Visible spectroscopy was used to determine the pyrene content of the copolymers. A solution with a mass concentration of 0.05 g/L was prepared and the absorbance of this solution was measured. Applying the Beer-Lambert law ($A = \epsilon bc$ where A , ϵ , b , and c are the absorbance at 342 nm, the molar extinction coefficient of 1-pyrenemethanol at 342 nm in THF equal to 42,700 L.mol⁻¹.cm⁻¹, the cell path length, and the molar concentration of pyrene in the solution, respectively), c was determined. This concentration was divided by the mass concentration of 50 mg/L of the pyrene-labeled PBMA to obtain the pyrene content referred to as λ_{Py} , expressed in μmol of pyrene per gram of sample. The molar fraction of PyLM incorporated into the copolymer was determined by applying Equation 3-3, where M_{PyLM} and M_{BMA} are the molar masses of the PyLM and BMA, equal to 586.35 ($n = 6.5$) and 142.2 g/mol, respectively.

$$f_{Py} = \frac{MW_{BMA}}{\frac{\rho_{Poly}}{C} + MW_{BMA} - MW_{PyLM}} \quad (3-3)$$

The characteristics of the different latex particles that were prepared for the pyrene-labeled and unlabeled samples described in this thesis, and which were not crosslinked, are listed in Table 3-1. The solids content of the dispersions was ~ 0.01 g solids per g of emulsion.

Finally, the steady-state fluorescence spectra for the pyrene-labeled polymers were acquired in THF to verify that the spectral features of pyrene were not modified during the emulsion polymerization process. The samples were dissolved to give an absorbance of 0.1 at 344 nm, and the solutions were degassed with nitrogen. The four characteristic peaks of pyrene were observed as well as excimer formation, indicating that pyrene was covalently attached to the polymer. A sample fluorescence spectrum is shown in Figure 3-5 for PyEG_{6.5}-PBMA(2.8).

Table 3-1: Characteristics of Latexes Prepared via Emulsion Copolymerization of *n*-BuMA and PyLM.

PyLM	Sample name	Label %	M _n (kg/mol)	PDI	Diameter (nm)	Diameter PDI
PyEG _{7.4} MA	PyEG _{7.4} -PBMA(3.2)	3.2	320	2.6	110	0.07
None	UL-PBMA(3.2)	--	380	1.6	114	0.05
PyEG _{6.5} MA	PyEG _{6.5} -PBMA(2.8)	2.8	230	2.5	113	0.03
None	UL-PBMA(2.8)	--	240	2.4	116	0.02
PyEG ₄ MA	PyEG ₄ -PBMA(2.4)	2.4	51*	2.1	111	0.10
None	UL-PBMA(2.4)	--	94*	2.0	101	0.04

* Apparent molecular weight measured against polystyrene standards.

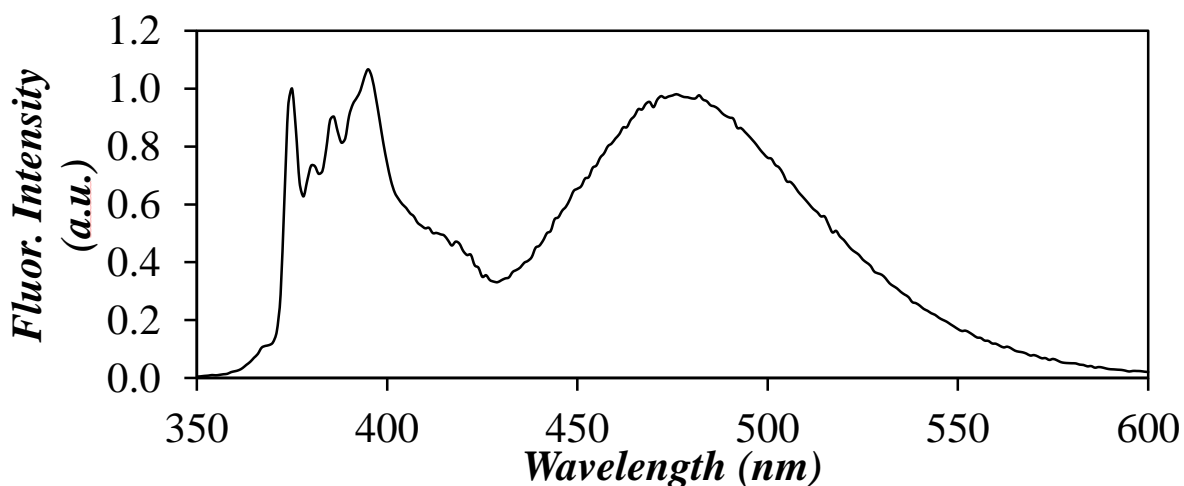


Figure 3-5: Fluorescence spectrum for PyEG_{6.5}-PBMA(2.8).

3.3 Polymerization Issues

3.3.1 Aggregation

As noted in Section 2.5, PyEG_nMA with $n > 6$ tended to disperse in aqueous solutions. It was expected that semi-batch emulsion polymerization would reduce the likelihood of PyLM aggregation into micelles. Ensuring that the rate of introduction of the PyLM into the reactor was lower than the

rate of PyLM consumption into the latex, only a small amount of PyLM would be in the batch reactor at any given time, keeping its concentration below its anticipated critical micellar concentration.

To investigate the effect that the polymerization method had on the distribution of the PyLMs in the copolymer, solution polymerization was conducted to obtain a pyrene-labeled PBMA (Py-PBMA) sample where the PyLMs would be incorporated randomly and with approximately the same pyrene content as in the emulsion polymerization. The polymerization was conducted to a conversion of less than 20%, to ensure minimal composition drift. The fluorescence decays obtained for the emulsion and solution polymerization products are compared in Figure 3-6. They were analyzed using the fluorescence blob model, which provides information about the level of pyrene clustering along the polymer from the molar fraction of aggregated pyrenes (f_{agg}), the rate of excimer formation from the product $k_{blob} \times N_{blob}$, where k_{blob} is the rate constant at which a pyrene label encounters another inside a blob, and N_{blob} represents the number of structural units in the volume of the polymer coil probed by an excited pyrene. The average lifetime $\langle \tau \rangle$ of the monomer decays was also determined by fitting the fluorescence decays with a sum of exponentials. The results from the decay analysis are shown in Table 3-2.

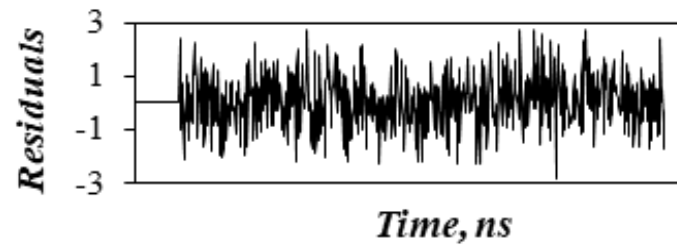
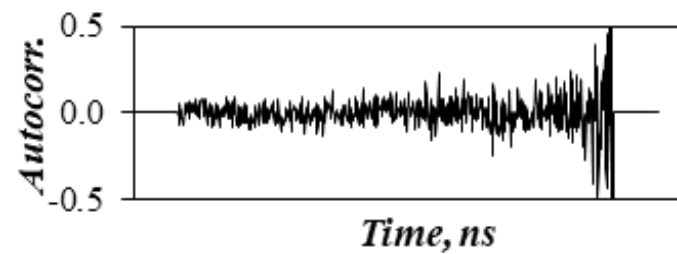
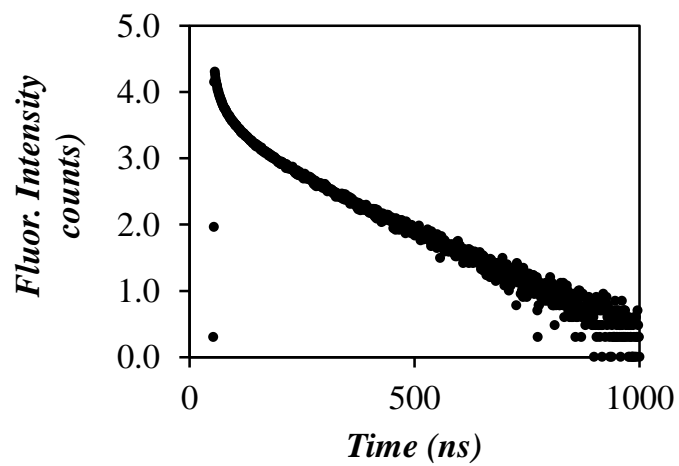
Table 3-2: Parameters f_{agg} , $k_{blob} \times N_{blob}$, and $\langle \tau \rangle$ retrieved from the decay analysis.

Polymerization Type	Labeling Percentage	f_{agg}	$k_{blob} \times N_{blob}$ (ns ⁻¹)	$\langle \tau \rangle$ (ns)
Emulsion	3.2 mol%	0.133	0.91	64
Solution	3.1 mol%	0.045	0.56	75

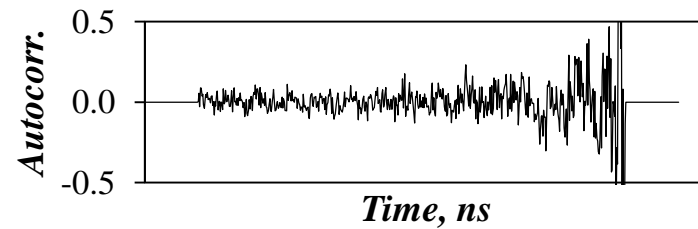
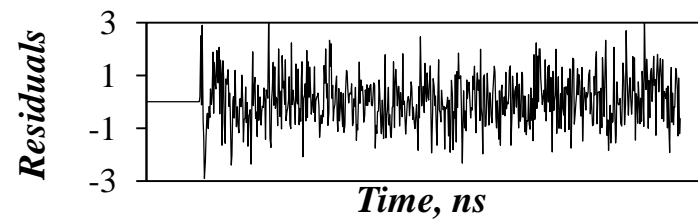
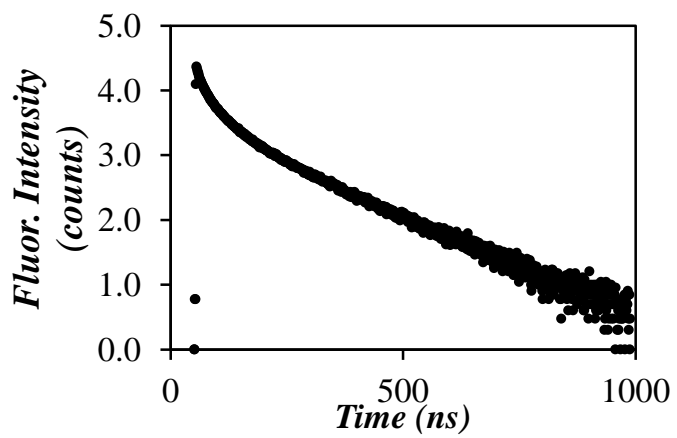
The 3-fold increase in f_{agg} , 1.6-fold increase in the product $k_{blob} \times N_{blob}$, and the 18% decrease in $\langle \tau \rangle$ all reflect higher aggregation and local concentration of the pyrene labels, and indicate that the

aggregation of the PyLMs seen in aqueous solution was not fully mitigated through the use of the semi-batch technique.

Emulsion
PyEG_{7.4}⁻
PBMA(3.2)
Monomer
Decay



Solution
(3.1%)
Monomer
Decay



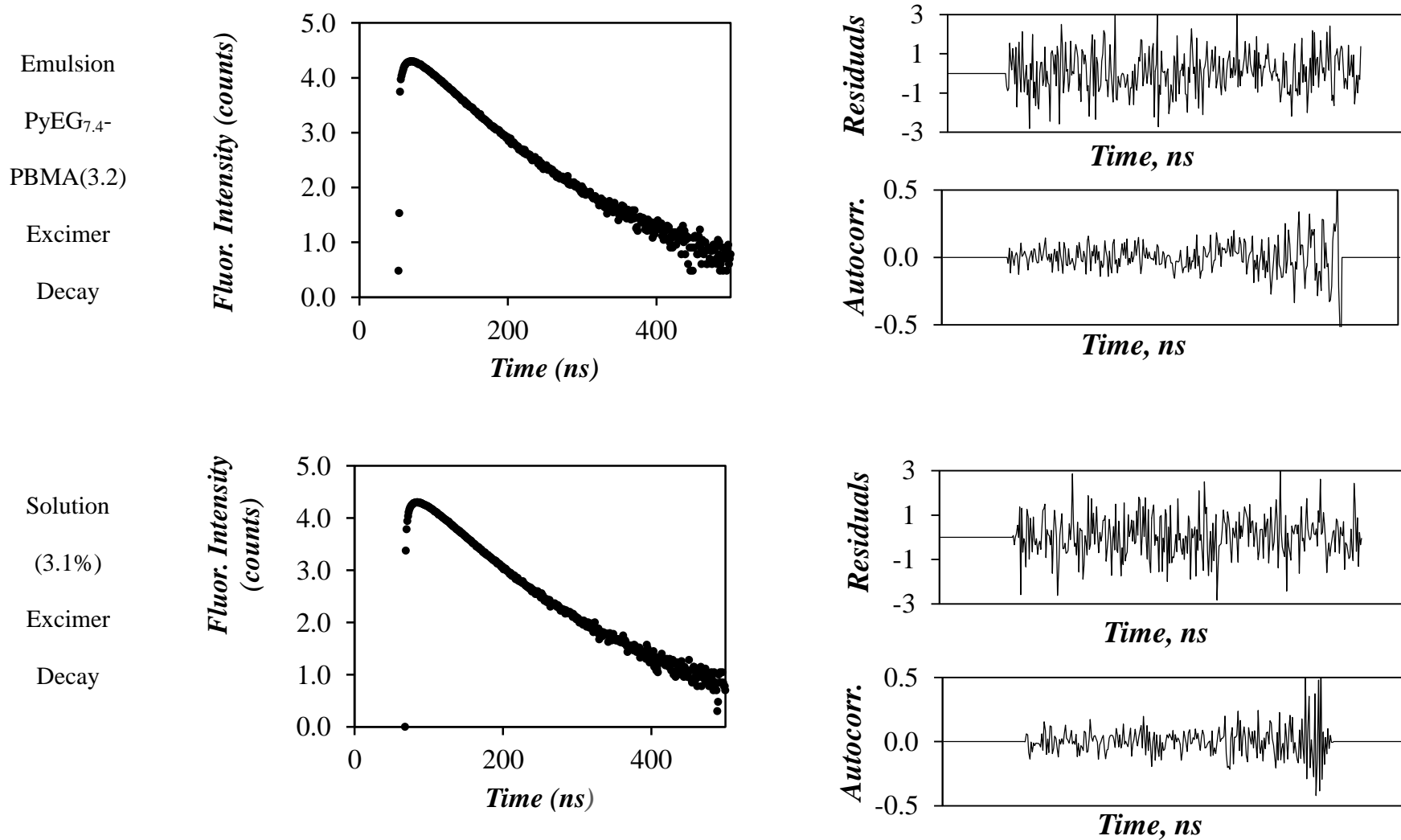


Figure 3-6: Time-resolved fluorescence decays for copolymers synthesized via solution and emulsion polymerization, with respective residuals and autocorrelation functions. Emulsion copolymerization yielded a steeper decay in the monomer, corresponding to more clustered pyrene molecules.

3.3.2 Pyrene Cleavage

Besides aggregation of the pyrene labels in the Py-PBMA samples prepared by emulsion copolymerization, further experiments uncovered that the pyrene labels could also be cleaved off during latex storage. This issue was identified as follows. While film annealing trials were underway, all the PyEG_{7,4}-PBMA(3.2) latex that had been dialyzed for the fluorescence measurements was used. Consequently, another batch of the latex dispersion was dialyzed. However, steady-state fluorescence showed that this newly-dialyzed polymer solution yielded significantly less excimer formation. Its pyrene content was measured by UV-Vis spectroscopy and found to have decreased from 3.2 mol% initially to 1.6 mol%, suggesting that the pyrene labels had been cleaved off from the polymer backbone. Upon further investigation, it was found that the pH of the dialyzed solution was neutral (~7.4) whereas the pH of the undialyzed solution was acidic (3-4). The acidic pH was assumed to be the cause of the cleavage, likely at the ester bond of the ethylene oxide linker. This also suggested that the PyLMs tended to concentrate at the particle surface, where they could be cleaved more easily by the acidic solution. The PyLM and emulsion copolymer were resynthesized, resulting in sample PyEG_{6,5}-PBMA(2.8), but immediately after the polymerization, an aliquot was dialyzed and the pH of the remaining solution was adjusted by addition of a phosphate buffer. Cleavage was no longer observed in the pH-adjusted dispersion.

3.4 Summary

PyLMs were copolymerized with *n*-butyl methacrylate by emulsion polymerization, to form latex particle dispersions. Dodecanethiol was used as a chain transfer agent to minimize crosslinking, which was initially observed for PyLMs prepared with an oligo(ethylene oxide) spacer with more than 5 ethylene oxide units. As the molecular weight and percentage incorporation of the PyLM increased, the T_g of the copolymer remained constant at 20 °C, a value similar to the T_g of neat

PBMA, demonstrating that the incorporation of the PyLM did not alter the glass transition of the copolymer. Several latex particle samples were prepared using PyEG₄MA, PyEG_{6.5}MA, and PyEG_{7.4}MA and yielded incorporation levels of 2.4, 2.8 and 3.2 mol%, respectively. Native latex particles were also prepared alongside the labeled latex, with similar molecular weight distributions and particle sizes as shown in Table 3-1.

Several issues including pyrene aggregation and cleavage were observed over the course of these experiments. Although the use of a semi-batch system was expected to mitigate the effects of PyLM aggregation during emulsion polymerization, the fraction of pyrene labels that were aggregated in the Py-PBMA sample was found to be 3 times higher than in a randomly labeled copolymer synthesized via homogenous solution polymerization. Thus it was clear that pyrene aggregation was not fully eliminated during semi-batch emulsion copolymerization. Pyrene cleavage was also detected when the Py-PBMA latex dispersions were not dialyzed, due to the acidic conditions generated. This problem was eliminated through pH adjustment of the dispersion.

Chapter 4

Film Formation

The particles synthesized in Chapter 3 were used in the study of IPD taking place during film formation. Steady-state fluorescence was applied to study the diffusion of the polymer chains across the boundaries of the latex particles. The I_E/I_M ratio obtained from the steady-state fluorescence spectra acquired over the course of film annealing was monitored as a function of annealing time as described in Section 1.3.3. Having consistently reached a higher level of pyrene incorporation in the Py-PBMA latex as compared to what had been achieved earlier, these new latex samples were expected to generate a much stronger excimer signal that would facilitate detection in the fluorometer and, consequently, the characterization of IPD taking place during latex film formation. The annealing trials were conducted at different annealing temperatures and profiles showing the fraction of mixing as a function of annealing time were constructed. A Fickian diffusion model was applied to determine the diffusion coefficients. This part of the study ensured that IPD could be characterized quantitatively, although the annealing process could also be characterized more qualitatively by monitoring the color change experienced by the latex film. In addition, the problems associated with PyLM aggregation described in Chapters 2 and 3 are further discussed in the present chapter.

4.1 Experimental

A mixture of the Py-PBMA (5 wt%) and unlabeled PBMA (95 wt%) latex was prepared. The latex particles had similar molecular weights ($M_n = 260$ and 230 kg/mol) and particle diameters ($D_h = 113$ and 116 nm) for the PyEG_{6.5}-PBMA(2.8) and unlabeled PBMA latex, respectively. The latex mixture (0.75 g) was deposited inside a quartz rectangular tube that was sealed with a rubber septum poked with two needles, one of them being connected to nitrogen gas and the other allowing nitrogen to flow through. The film was dried in the dark overnight to ensure the complete removal of water.

The latex film was prepared on one of the inner walls of a sealed tube and under a nitrogen atmosphere instead of the quartz plates that had been used earlier¹² to prevent photobleaching that was found to occur with PyEG_{7.4}-PBMA(3.4). The tube was submerged in a heated oil bath for a requisite amount of time. Once the desired time had elapsed, the tube was removed and submerged in an oil bath at room temperature to cool it rapidly. The oil was removed and the outer walls of the tube were cleaned with acetone, followed by fluorescence-grade THF. The fluorescence spectrum of the annealed film was acquired and its I_E/I_M ratio was calculated. This process was repeated over the course of a day at increasing time intervals.

To simulate complete annealing that would occur after an infinite annealing time ($t = \infty$) and would result in a fully homogeneous film, the film was dissolved in THF, redeposited in the tube and dried. The resulting film was placed in the oil bath for one hour to ensure complete annealing and its fluorescence spectrum was acquired to obtain $I_E/I_M(t = \infty)$.

The fraction of mixing (f_m) was determined from the I_E/I_M ratio using Equation 4-1.

$$f_m = \frac{\frac{I_E}{I_M} - \frac{I_E}{I_M} \Big|_{t=0}}{\frac{I_E}{I_M} - \frac{I_E}{I_M} \Big|_{t=\infty}} \quad (4-1)$$

As described in Equations 1-11 and 1-12, the fraction of mixing can be used in tandem with Fick's law to determine the diffusion coefficient of the polymers undergoing IPD in the films.

4.2 Steady-State Fluorescence

The steady state fluorescence spectra were acquired by exciting the films at 344 nm (Figure 4-1). The fluorescence signal was recorded from 350 nm to 650 nm at 1 nm intervals and a scan rate of 10 nm.s⁻¹ using the front-face geometry. The I_E/I_M ratio was calculated by dividing the integral of the fluorescence signal from 500 to 530 nm for I_E over that from 392 to 398 nm for I_M . The fluorescence signal of the first peak in the monomer fluorescence spectrum at 375 nm is typically selected to measure the I_M intensity, to avoid interference with the excimer fluorescence. Since excimer formation was expected to be low in the solid latex films, the excimer fluorescence could not interfere much with the fluorescence of the pyrene monomer. Furthermore, the pyrene labels in the Py-PBMA films could reabsorb the fluorescence emitted at 375 nm, which would reduce the I_M intensity.

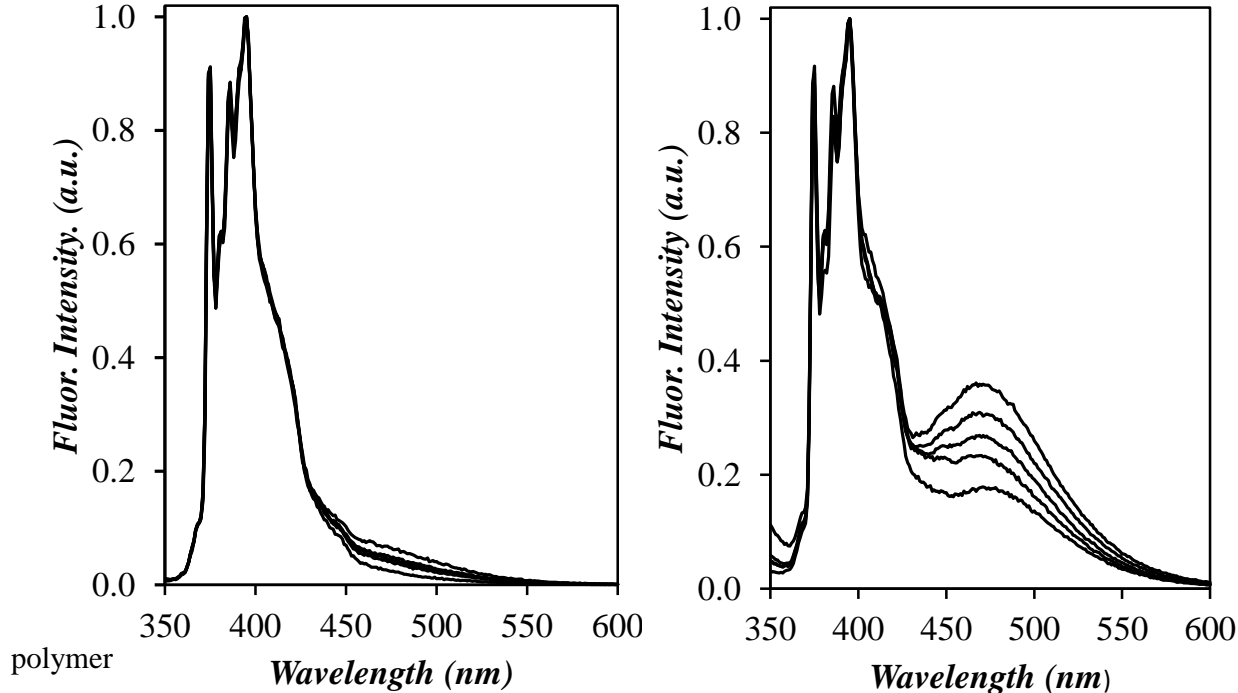
Since reabsorption increases with the number of pyrene labels present in the film, the fluorescence intensity of the first peak at 375 nm was expected to decrease for increasing film thickness, thus resulting in fluorescence intensities that would vary with film thickness. Selection of the fourth peak at 395 nm for I_M ensured that its intensity relatively to that of the excimer would be unaffected by film thickness.

The above discussion assumes that excimer formation would be reduced in the solid film, as observed earlier.¹² However the higher pyrene content of the Py-PBMA latexes resulted in stronger excimer emission. Thus in the end, no peak was deemed ideal to determine I_M . Consequently, the analysis was attempted by taking I_M from the monomer fluorescence peaks at both 375 and 398 nm, but the I_M value obtained at 375 nm was found to yield more consistent results.

As shown in Figure 4-1B, the PyEG_{6.5}-PBMA(2.8) sample yielded substantially more excimer in the solid latex films at different annealing times than sample PyEG₃-PBMA(1.9), also shown in Figure 4-1A for comparison. In fact, the enhancement in excimer fluorescence is significant, considering that a 47% enhancement in pyrene content from 1.9 to 2.8 mol% resulted in a 5-fold increase in the I_E/I_M ratio. Since pyrene excimer formation in the solid state results from an equilibrium between isolated and clustered pyrene labels (see Figure 1-6), a 47% increase in pyrene content would be expected to yield a 47% increase in the I_E/I_M ratio rather than the much larger 540% increase observed experimentally. This discrepancy is most likely due to the presence of pyrene clusters in the latex particles that artificially increase their ability to form excimer. This conclusion would be in line with the observations made in Chapter 2 that the PyEG_n-MA monomers formed micelles in aqueous solution, that would lead to their blocky incorporation during emulsion copolymerization.

Clustering is also evident when considering the I_E/I_M ratio obtained at infinite annealing time, which equaled 0.39 (± 0.06) and 0.027 (± 0.005) for the PyEG_{6.5}-PBMA(2.8) and PyEG₃-PBMA(1.9) latex particles, respectively. Under these infinite dilution conditions that should minimize excimer formation, I_E/I_M for PyEG_{6.5}-PBMA(2.8) was more than 10 times larger than for PyEG₃-PBMA(1.9), providing strong support for the presence of pyrene clusters in the particles prepared with PyLMs having a longer EG_n spacer. Furthermore the range of I_E/I_M values spanning the annealing process was narrower for PyEG_{6.5}-PBMA(2.8). Indeed, I_E/I_M averaged over all temperatures was found to decrease by 54 (± 8) % and 78 (± 3) % from zero ($t_{an} = 0$) to infinite ($t_{an} = \infty$) annealing time for the latex films prepared with the PyEG_{6.5}-PBMA(2.8) and PyEG₃-PBMA(1.9) latex particles, respectively. The inability of the PyEG_{6.5}-PBMA(2.8) sample to reach as low I_E/I_M values as the PyEG₃-PBMA(1.9) sample at infinite annealing time is a clear indication that the pyrene labels are not homogeneously distributed in the latex film at $t_{an} = \infty$. While the increase in the I_E/I_M ratio

observed for PyEG_{6.5}-PBMA(2.8) facilitates the detection of excimer fluorescence, the reduced span of I_E/I_M values as a function of t_{an} for this sample, combined with the existence of pyrene clusters in the



polymer matrix, will most certainly complicate the analysis of the I_E/I_M ratios for the characterization of IPD.

A)

B)

Figure 4-1: Steady-state fluorescence spectra for A) PyEG₃-PBMA(1.9)labeled and B) 2.8% PyEG_{6.5}-PBMA(2.8)-labeled films at T = 100°C at different annealing times.

The steady-state fluorescence spectra shown in Figure 4-1 were used to determine the I_E/I_M ratios that were applied to calculate the fraction of mixing (f_m) according to Equation 1-13, which

was plotted as a function of time in Figure 4-2. The overall fraction of mixing profile was consistent with the results reported by Casier.¹² A rapid increase was observed initially, as shorter chains diffused out of the particles, before approaching unity at infinite time at a reduced rate, corresponding to the diffusion of the longer chains. It should be noted that the PyEG_{6.5}-PBMA(2.8) polymer diffused significantly faster than the PyEG₃-PBMA(1.9) polymer of similar molecular weight. This result was surprising, as IPD should not depend on the nature of the PyLM (PyEG_{6.5}MA versus PyEG₃MA) or the pyrene content (2.8 versus 1.9 mol%).

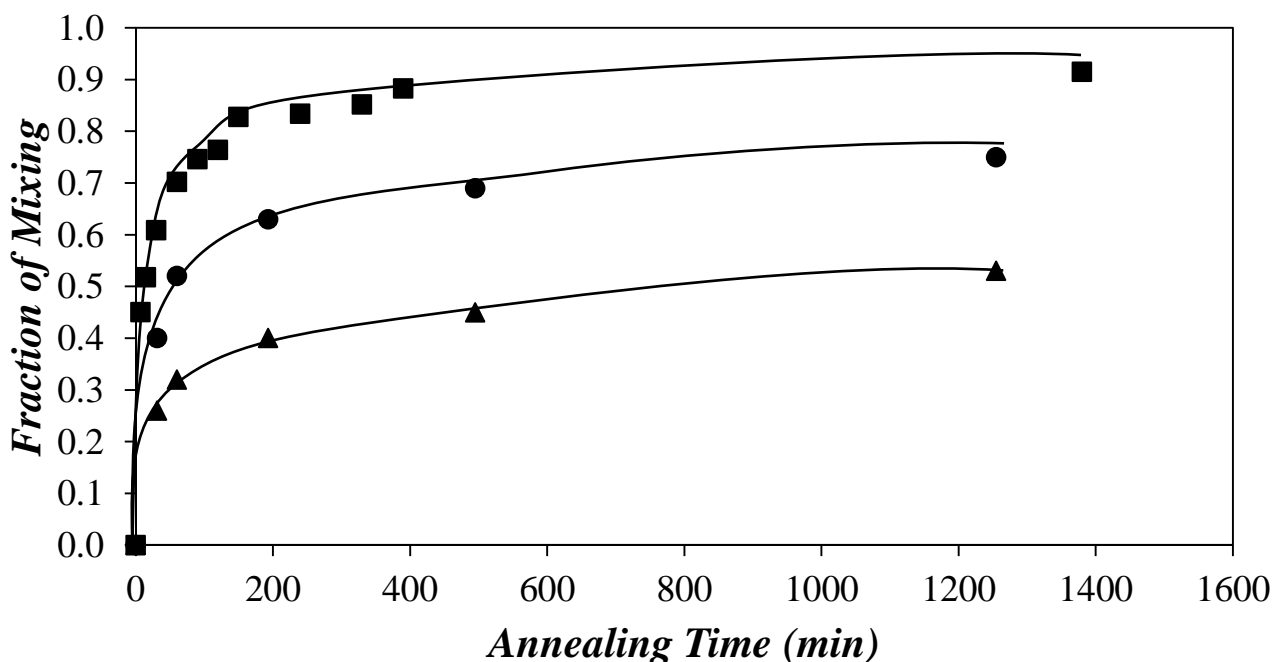


Figure 4-2: Fraction of mixing as a function of annealing time at T = 90 °C for (■) PyEG_{6.5}-PBMA(2.8) (230 kg/mol), (▲) PyEG₃-PBMA(1.9) (430 kg/mol), and (●) PyEG₃-PBMA(1.9) (200 kg/mol). PyEG_{6.5}-PBMA(2.8) is seen to diffuse much more quickly in the first 2 hours of annealing.

4.2.1 Photobleaching

While the f_m -versus- t_{an} trends shown in Figure 4-2 exhibit the same features that were reported earlier,¹² several inconsistencies were encountered in the current project due to a number of

experimental problems. The first issue discussed in this section was the observation that the films underwent photobleaching. When the latex solutions were cast on a quartz plate to prepare the films as was done earlier,¹² inspection of the films under UV light showed evidence of photobleaching as shown in Figure 4-3. A rectangle with a different shade of color appeared on the film where it had been irradiated. In fact, the outline of the photobleached rectangle in the films became even more pronounced for increasing irradiation time. This was further investigated through steady-state fluorescence, by monitoring the I_E/I_M ratio as a function of irradiation time. A 10% reduction in the I_E/I_M ratio was observed over an irradiation period of 10 minutes. This result suggested that the I_E/I_M ratio used to determine the fraction of mixing would drift as a function of irradiation time, and thus with each spectrum acquisition conducted over the course of film annealing. A solution to this problem was implemented by casting the film in a quartz tube sealed with a rubber septum and kept under nitrogen during film annealing. This new experimental setup eliminated photobleaching, as can be seen in Figure 4-4.

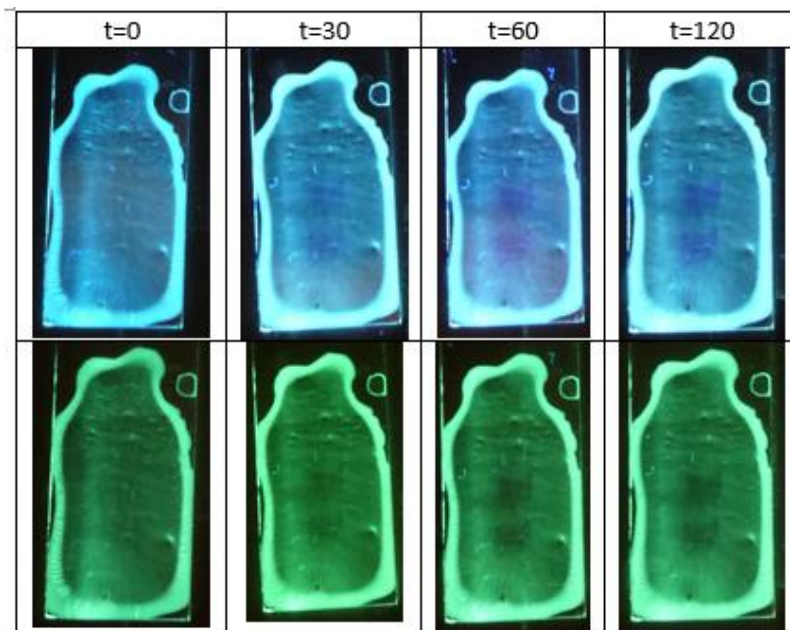


Figure 4-3: Latex films (5% PyEG_{7,4}-PBMA(3.2), 95% native PBMA) cast on a quartz plate and irradiated for different time periods in the fluorometer. The films were excited with a hand-held UV lamp and photographed either as-is (top) or through a 495 nm cut-off filter (bottom). The bleached rectangular area visible at the center of the film corresponds to the zone irradiated by the lamp of the fluorometer.

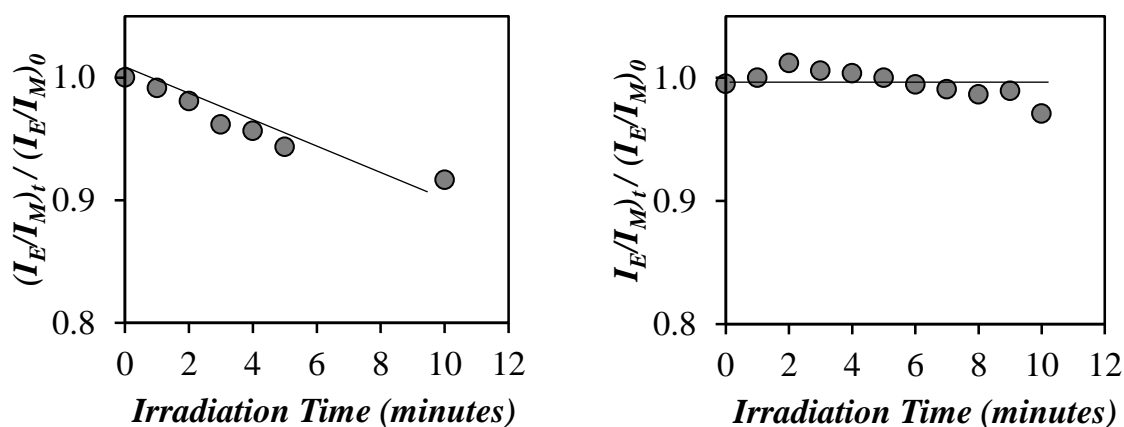


Figure 4-4: Plot of the I_E/I_M ratio normalized to $t_{an} = 0$ as a function of irradiation time. The latex film (5% PyEG_{7,4}-PBMA(3.2), 95% native PBMA) was cast (left) on a quartz plate and (right) on the wall of a square quartz tube that was kept under nitrogen atmosphere.

Other methods to reduce degradation of the latex films by photobleaching were investigated. Decreasing the intensity of the incident beam did decrease the amount of photobleaching to ~6% over 10 minutes, however this smaller change in I_E/I_M ratio was still deemed too large for the calculation of the f_m values. Neutral density filters were also employed to decrease the overall lamp intensity on the irradiated area, but no decrease in photobleaching was observed. Finally, hydroquinone was added to the latex dispersion used to cast the films. If the decrease in fluorescence intensity in the irradiated area of the film was due to homolytic cleavage of the oligo(ethylene glycol)

linker of the pyrene labels, hydroquinone was expected to act as a radical scavenger that might reduce this effect. Unfortunately, no improvement was observed.

Therefore, the only efficient method to prevent photobleaching of the latex films was by casting them on the inner wall of a quartz tube, and keeping the film under nitrogen during the acquisition of the fluorescence spectrum. Consequently, all the fluorescence data for the latex films reported in this thesis were obtained using this methodology.

4.2.2 Other Complications Encountered in the Characterization of IPD by Steady-State Fluorescence

Having resolved the photobleaching problem through the use of a quartz tube to cast the latex films, the fluorescence experiments could start in earnest whereby the fluorescence spectra for the latex films were acquired at different annealing times and temperatures. Unfortunately, the analysis of the fluorescence data led to other inconsistencies. First, the I_E/I_M ratios determined at $t_{an} = 0$ at three different positions on a same film showed up to 12% variation from the average I_E/I_M value, and up to 22% difference between films. Since $(I_E/I_M)(t_{an}=0)$ appears in the calculation of all the f_m values as shown in Equation 1-13, a 12% variation in the initial I_E/I_M value for the same film was bound to have a detrimental effect on the f_m -versus- t_{an} trends used to characterize IPD. Second, the I_E/I_M ratios obtained at three different positions on the same film at $t_{an} = \infty$ were more similar, showing variations of less than 3%, but varied substantially from film to film with differences of up to 43%. Sample results illustrating these observations are shown in Table 4-1.

Table 4-1: I_E/I_M at $t_{an} = 0$ and $t_{an} = \infty$ obtained from fluorescence spectra acquired at three different spots on three films (5% PyEG_{6.5}-PBMA(2.8), 95% PBMA), annealed at three different temperatures.

I_E/I_M	Trial 1 (T = 100°C)	Trial 2 (T = 105°C)	Trial 3 (T=115°C)
-----------	---------------------	---------------------	-------------------

Spot 1 at $t = 0$	0.89	0.96	0.89
Spot 2 at $t = 0$	1.16	0.91	0.79
Spot 3 at $t = 0$	0.99	1.03	--
Spot 1 at $t = \infty$	0.35	0.46	0.41
Spot 2 at $t = \infty$	0.37	0.48	0.40
Spot 3 at $t = \infty$	0.36	0.50	--

A third problem was the observation that the I_E/I_M ratio decreased very rapidly over the first seven minutes of annealing, suggesting that the pyrene labels underwent rapid dilution, especially in comparison to the overall decrease in I_E/I_M over the course of the whole annealing process. This effect is illustrated in Table 4-2, where the decrease in the I_E/I_M ratio over the first 7 minutes of annealing represented 44 (± 2) % of the decrease in I_E/I_M observed over the entire annealing process (note: Sample *e* was excluded from these calculations, as it is a clear outlier). Although Casier did not perform his annealing trials at exactly 100 °C, two trials were conducted at 98 °C and 102 °C. Reductions of 23.1% and 23.6% over the first 7 minutes of annealing were observed in the PyEG₃-PBMA(1.8), respectively.

Table 4-2: Representative I_E/I_M values at $t_{an} = 0$ and 7 min at $T = 100^\circ\text{C}$, and decrease in I_E/I_M over the first 7 min and after complete mixing ($t_{an} = \infty$) for latex film (5% PyEG_{6.5}-PBMA(2.8) and 95% native PBMA)

I_E/I_M	a	b	c	d	e
$t = 0$	0.89	1.16	0.99	0.85	0.75
$t = 7$	0.66	0.79	0.71	0.63	0.61
$\Delta I_E/I_M$ t_0 to t_7	0.23	0.37	0.28	0.22	0.14

$\Delta I_E/I_M$ t_7 to t_∞	0.31	0.42	0.35	0.27	0.38
--------------------------------------	------	------	------	------	------

Rapid mixing of the pyrene labels in the early annealing stage and the poor reproducibility of the experiments could be explained by the presence of a plasticizer facilitating the IPD of the Py-PBMA chains. As explained earlier, the particles were dialyzed against a mixture of water, ethanol and surfactant to remove the CTA, initiator, and unreacted monomer which could potentially act as plasticizers. But since the PyEG_{6.5}MA monomer was significantly more hydrophilic than PyEG₃MA, water might be retained in the PyLM aggregates whose existence was inferred throughout this thesis. Once the pyrene-labeled latex is incorporated in the film, water could diffuse into the film and act as a plasticizer. Instead of drying the films overnight, they were dried over a period of several days in an attempt to remove additional water. Unfortunately, the same inconsistent results were obtained.

The very rapid decrease in I_E/I_M observed during annealing of the films prepared with the PyEG_{6.5}-PBMA(2.8) latex could be rationalized if a large fraction of the pyrene labels were concentrated near the surface of the latex particles. This arrangement of the PyEG_n-MA monomers in the fluorescently labeled latex would be compatible with the higher hydrophilicity of these monomers. As mentioned earlier, their ability to form micelles in aqueous solution is expected to lead to their blocky incorporation into the Py-PBMA chains, which would generate hydrophilic microdomains made of oligo(ethylene oxide) segments in the hydrophobic PBMA latex that would tend to distribute themselves closer to the particle interface with the aqueous phase. In turn, the preferred location of the oligo(ethylene oxide) spacers bearing the pyrene labels near the surface of the particles could explain other experimental problems encountered in this study. Pyrene labels located near the surface of the particles should indeed be more sensitive to cleavage, degradation, and rapid diffusion in the latex film.

In an effort to characterize the distribution of pyrene labels within the latex particles, a fluorescence quenching study was conducted with nitromethane. Being water-soluble, nitromethane would quench preferentially pyrene labels located near the surface of the latex particles. If the composition of the particle surface were similar to that of the particle interior, quenching of the pyrene fluorescence by nitromethane should yield an overall decrease in fluorescence intensity without affecting the shape of the fluorescence spectrum. If more pyrene labels were located at the particle surface however, more pyrene excimer would be generated at the particle surface than in the particle interior. Quenching of the pyrene labels near the surface would reduce excimer emission at the particle surface, leaving only a weaker excimer emission from the interior of the particles. Thus quenching of the surface of a latex particles with a heterogeneous distribution of pyrene labels would result in a decrease in the overall fluorescence intensity, but a larger decrease in the excimer emission intensity. To this end, an aqueous dispersion of the pyrene-labeled particles with an absorbance of 0.1 at 342 nm was mixed with increasing concentrations of nitromethane, while monitoring the monomer intensity (I_M) and the I_E/I_M ratio. The quenching experiments were conducted with the PyEG_{6.5}MA- and PyEG₃MA-labeled particles and the results are compared in Figures 4-5 and 4-6.

Upon adding nitromethane the intensity of the fluorescence spectra was strongly reduced (see Figure 4-5), demonstrating efficient quenching of the pyrene labels by nitromethane. The pyrene monomer was quenched with the same efficiency for both particles as shown in Figure 4-5C. However, changes in the shape of the normalized fluorescence spectra are clearly visible for the PyEG_{6.5}-PBMA(2.8) latex particles, while hardly any change is observed for PyEG₃-PBMA(1.9). This is reflected in Figure 4.6C, where the I_E/I_M ratio normalized to its value in the absence of nitromethane remained close to unity for the PyEG₃-PBMA(1.9) particles but decreased for PyEG_{6.5}-PBMA(2.8). The decrease in I_E/I_M for the latex particles prepared with the more hydrophilic PyEG_{6.5}-MA monomer demonstrates that more excimer was generated at the surface than in the interior of the

particles. Consequently, these fluorescence quenching experiments suggest that the PyEG_{6.5}-MA monomer was not homogeneously distributed in the latex particles, but rather resided preferentially near the particle surface. This interpretation of the quenching results agrees with many of the observations made so far, and in particular provides a rationale for the many experimental problems experienced throughout this project. Most importantly, the Fickian diffusion model used to interpret the f_m -versus- t_{an} trends cannot be applied, since it assumes a homogenous distribution of PyLM throughout the latex particles.

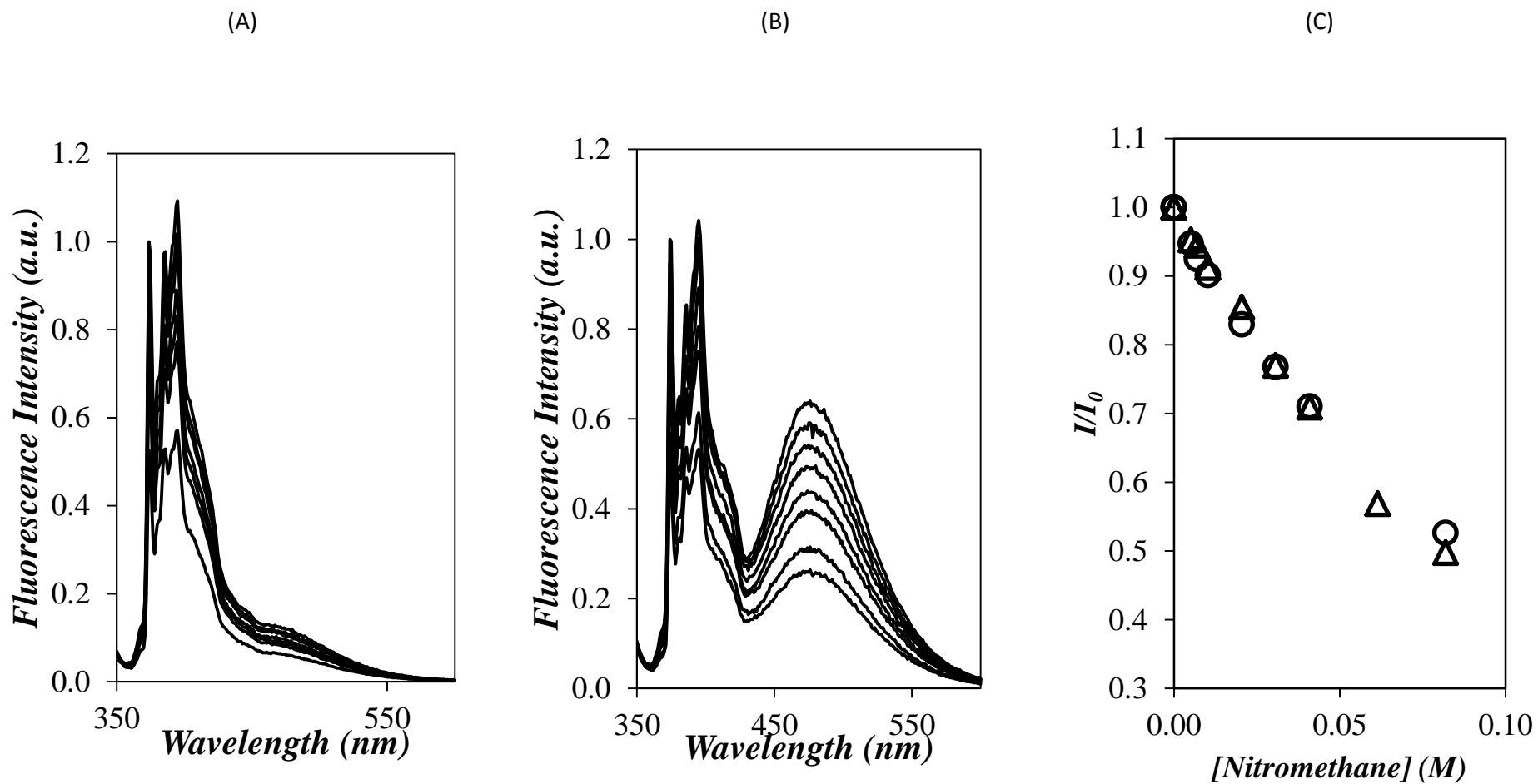


Figure 4-5: Fluorescence spectra for A) PyEG₃-PBMA(1.9) and B) PyEG_{6.5}-PBMA(2.8) latex particles at increasing concentrations of nitromethane. (C)

Normalized fluorescence intensity of the pyrene monomer for (○) PyEG₃-PBMA(1.9) and (△) PyEG_{6.5}-PBMA(2.8) latex particles as a function of the nitromethane concentration.

(A)

(B)

(C)

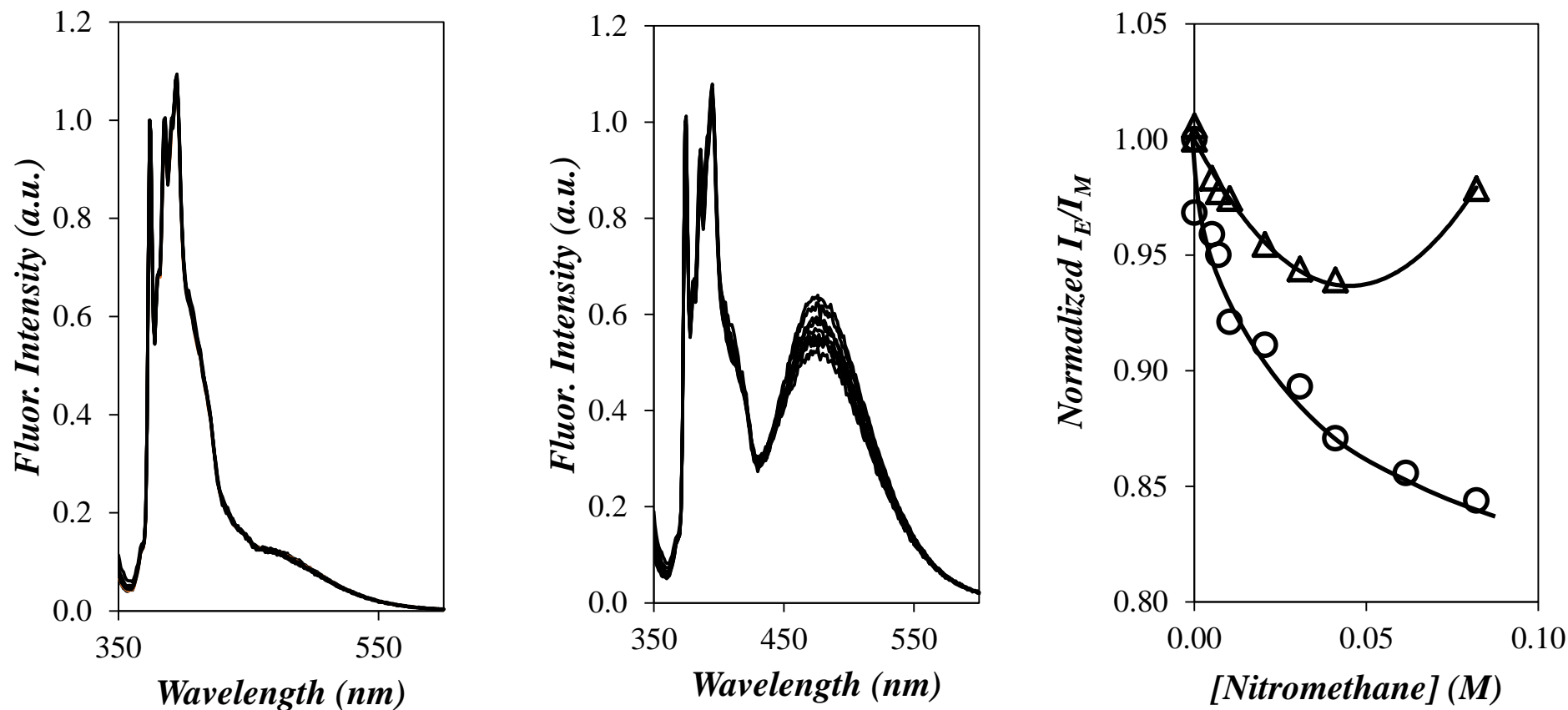






Figure 4-6: Fluorescence spectra for the A) PyEG_{6.5}-PBMA(2.8) and B) PyEG₃-PBMA(1.9) latex particles normalized at 375 nm, (C) Normalized I_E/I_M ratio for (○) PyEG₃-PBMA(1.9) and (△) PyEG_{6.5}-PBMA(2.8) latex particles as a function of the nitromethane concentration.

4.2.3 Film Color Change

It was shown by Casier that IPD could be followed by monitoring the change in film color. The concomitant decrease and increase in, respectively, excimer and monomer emission taking place during film formation resulted in a color change from light green to purple-blue. The change was more obvious when visualized with a 475 nm cut-off filter, where only the excimer fluorescence was observed. With the cut-off filter, the color changed from green to almost colorless.

Since films prepared with PyEG_{6.5}-PBMA(2.8) generated more excimer (emitting in the green region) than films prepared with the PyEG₃-PBMA(1.9) latex, the initial color of the former films showed a stronger green fluorescence. Unfortunately, as compared to the film prepared with PyEG₃-PBMA(1.9), the color change in the PyEG_{6.5}-MA-labeled films was not significant. The weaker color change observed for PyEG_{6.5}-PBMA(2.8) films is compared to Casier's films in Tables 4-3 and 4-4.

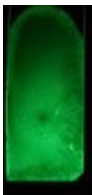




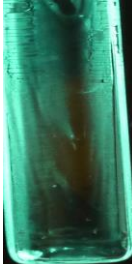
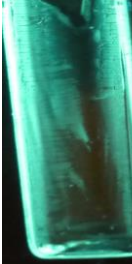

Table 4-3: Pictures for PyEG₃MA- and PyEG_{6.5}MA-labeled film mixtures annealed at 75 °C and excited with long-wavelength UV light (no cut-off filter applied).

	$f_m = 0$	$f_m = 0.3$	$f_m = 0.7$	$f_m = 1$
PyEG ₃ MA				



The lack of change in color of the fluorescent films as a function of annealing time when the PyEG_{6.5}-PBMA(2.8) latex particles were used provides additional evidence that the pyrene labels were clustered in the Py-PBMA chains constituting the latex. The main effect of pyrene label clustering is that even under conditions where the film is fully annealed, the pyrene clusters still form excimer efficiently, and thus continue emitting in the green region regardless of the extent of annealing. As a result, the films prepared with the PyEG_{6.5}-PBMA(2.8) latex were deemed unsuitable to monitor film annealing.

Table 4-4: Pictures for PyEG₃MA- and PyEG_{6.5}MA-labeled films annealed at 75 °C and excited with long-wavelength UV light (with 475 nm cut-off filter).

	$f_m = 0$	$f_m = 0.3$	$f_m = 0.7$	$f_m = 1$
PyEG ₃ MA				
PyEG _{6.5} MA				

4.3 Summary

Latex dispersions were initially cast onto quartz plates to prepare the films, but photobleaching made it necessary to anneal the films under nitrogen. To avoid this problem, it was determined that the films could be prepared in a square quartz tube sealed with a rubber septum and maintained under nitrogen. Steady-state fluorescence was used to monitor film formation over time. Although there was a significant increase in the I_E/I_M ratio for the PyEG_{6.5}-PBMA(2.8) sample ($I_E/I_M = 1.0$) as compared to PyEG₃-PBMA(1.9) ($I_E/I_M = 0.1$), the span of I_E/I_M values observed over the course of annealing was significantly smaller for the film that yielded the larger I_E/I_M ratio.

Aside from the photobleaching issue, I_E/I_M at $t_{\text{an}} = 0$ was found to vary significantly when determined at different spots on the same film, and also for different films having the same composition. Furthermore, I_E/I_M exhibited a sharp decrease at early annealing times from 0 to 7 minutes, indicating rapid dilution of the pyrene labels. These results were attributed, in part, to a heterogeneous distribution of pyrene labels in the particles, with PyEG_n-MA monomers clustering at their surface. This was confirmed by conducting a fluorescence quenching study of the pyrene-labeled latex particles in aqueous dispersions. Since the Fickian model used to monitor IPD of the Py-PBMA chains across the latex particle boundaries assumed a homogeneous distribution of pyrene labels within the particles, a high concentration of pyrene clusters at the particle surface implies that an analysis of IPD based on the Fickian model is not feasible at the present time.

Chapter 5

Summary and Discussion

Over the course of the project, PyLMs with ethylene glycol linker lengths of 4, 6.5, and 7.4 units were synthesized and successfully copolymerized with *n*-butyl methacrylate. Ethoxylated pyrenemethanol was initially synthesized in two different ways: by anionic polymerization, and through a coupling method. The coupling substrate originally used was 1-bromomethylpyrene, but the product obtained was shown to have two significant lifetimes in the time-resolved fluorescence spectrum. A tosylation method was introduced instead, yielding ethoxylated 1-pyrenemethanol with over 90% of one lifetime component. Acylation of the ethoxylated pyrene to obtain the PyLM in high yield and purity was confirmed by several analysis techniques including ^1H NMR and fluorescence spectroscopy. Copolymerization of the PyLM was successful upon addition of dodecanethiol to

minimize crosslinking, and the PyLMs were incorporated at 2.4, 2.8 and 3.2% for $n = 4$, 6.5, and 7.4, respectively. This was a significant improvement from the 1.9% incorporation achieved by Casier for PyEG₃MA.

Many issues arose in the synthesis of the monomer and the latex particles. The first problem noted was micellization of the PyLM for $n = 6.5$ and 7.4. Micellization of the PyLM apparently resulted in aggregation of the pyrene labels in the polymer. It was hoped that a semi-batch process could minimize label clustering, by operating under starved conditions such that all the monomer would be added into the copolymer as it was fed into the reaction.

Since aggregation was thought to have been mitigated by the semi-batch process, the polymer was tested for aggregation using the fluorescence blob model, by comparing the copolymer synthesized via emulsion polymerization with a polymer synthesized by solution polymerization. It was found that the molar fraction of aggregated pyrenes was three times higher for the polymer synthesized by emulsion polymerization. This pyrene-labeled latex was nevertheless used in the annealing experiments, as it was thought that the aggregated polymer would only yield a larger I_E/I_M value at $t = \infty$.

Another issue arising with emulsion polymerization was cleavage of the pyrene labels from the polymer in undialyzed emulsions. The undialyzed emulsions were found to have a pH around 3 – 4, whereas the dialyzed samples were close to neutral. The pH differences and label cleavage were observed in pyrene-containing emulsions for all linker lengths, including those synthesized by Casier. Immediate dialysis or pH adjustment of these emulsions was necessary to avoid this problem.

After the issues associated with the monomer and particle synthesis were thought to have been resolved, film formation investigations were initiated but problems arose again. Photobleaching was visually observed after UV irradiation of the films in the fluorometer, and confirmed through

steady-state fluorescence measurements. Although a number of modifications were attempted, producing and annealing the films under nitrogen was found to best reduce photobleaching.

The initial results from steady-state fluorescence looked promising, as the film showed significantly more excimer formation as compared to Casier's. However, the I_E/I_M ratio did not decrease much with increasing annealing time. Overall, the film prepared with the PyEG_{6.5}-PBMA(2.8) sample yielded an overall reduction in I_E/I_M from a zero-to-infinite annealing time of about 40%, whereas the film prepared with Casier's PyEG₃-PBMA(1.9) sample showed a decrease of over 75%. The smaller decrease in I_E/I_M obtained for the film prepared with the PyEG_{6.5}-PBMA latex resulted in no clear color change for the film during annealing.

Furthermore, the I_E/I_M measurements were inconsistent, with values at $t_{an} = 0$ ranging from 0.75 to 1.10 for different films prepared with the same pyrene-labeled latex. These inconsistencies were observed even for the same film measured at different spots. Rapid dilution of the pyrene labels was also observed from $t_{an} = 0$ to 7 min. This was attributed to pyrene aggregation at the surface of the particles, and therefore to a non-homogenous distribution of PyLM throughout the pyrene-labeled latex particles. This was confirmed through a quenching study with nitromethane.

The inhomogeneous PyLM distribution resulted in f_m -versus- t_{an} profiles which were inconsistent for repeat trials. Additionally, without homogenous distribution of the PyLM, it was impossible to use a Fickian diffusion model to calculate the diffusion coefficients.

Given all the issues encountered in the monomer synthesis, preparation of the pyrene-labeled latex, and film preparation, combined with inconsistent and unreliable results, it would be advisable not to use the PyEG_{6.5}-PBMA(2.8) or PyEG_{7.4}-PBMA(3.2) particles in film formation studies. The only PyLM that did not seem to result in aggregation was PyEG₄MA, although PyEG₅MA was not studied. Aggregation of the PyLM in water is clearly a limiting factor in this project. It is likely that n

= 4 or 5 represents the largest oligo(ethylene oxide) linker that can be used to prepare a PyLM to synthesize pyrene-labeled latex particles with a homogenous pyrene label distribution within the latex particles.

References

1. Gauthier, C.; Guyot, A.; Perez, J.; Sindt, O. Film Formation and Mechanical Behavior of Polymer Laticies. *Film Formation in Waterborne Coatings*, American Chemical Society: Washington, DC, **1996**, Chapter 10, pp 163 – 178.
2. Winnik, M. A. Latex Film Formation. *Current Opin. Colloid Interface Sci.* **1997**, 2, 192-199.
3. Eckersley, S. T.; Rudin, A. Film Formation of Acrylic Copolymer Laticies: A Model of Stage II Film Formation. *Film Formation in Waterborne Coatings*, American Chemical Society: Washington, DC, **1996**, Chapter 1, pp 2 – 21.
4. Wang, Y.; Winnik, M. A. Polymer Diffusion Across Interfaces in Latex Films. *J. Phys. Chem.* **1993**, 97, 2507-2515.
5. Zhao, C.; Wang, Y.; Hruska, Z.; Winnik, M. A. Molecular Aspects of Latex Film Formation: An Energy-Transfer Study. *Macromolecules* **1990**, 23, 4082-4087.
6. Wang, Y.; Winnik, M. A. Energy-Transfer Study of Polymer Diffusion in Melt-Pressed Films of Poly(methyl methacrylate). *Macromolecules* **1993**, 26, 3147-3150.

7. Oh, J. K.; Tomba, P.; Ye, X.; Eley, R.; Radekacher, J.; Farwaha, R.; Winnik, M. A. Film Formation and Polymer Diffusion in Poly(vinyl acetate-*co*-butyl acrylate) Latex Films. Temperature Dependence. *Macromolecules* **2003**, *36*, 5804-5814.
8. Farinha, J. P. S.; Martinho, J. M. G.; Yekta, A.; Winnik, M. A. Direct Nonradiative Energy Transfer in Polymer Interphases: Fluorescence Decay Functions from Concentration Profiles Generated by Fickian Diffusion. *Macromolecules* **1995**, *28*, 6084-6088.
9. Kim, K. D.; Sperling, L. H.; Klein, A.; Wignall, G. D. Characterization of Film Formation from Direct Multi-emulsified Polystyrene Latex Particles via SANS. *Macromolecules* **1993**, *26*, 4624-4631.
10. Hahn, K.; Ley, G.; Schuller, H.; Oberthiir, R. On Particle Coalescence in Latex Films. *Colloid Polym. Sci.* **1986**, *264*, 1092-1096.
11. Yoo, J. N.; Sperling, L. H.; Glinks, C.J.; Klein, A. Characterization of Film Formation from Polystyrene Latex Particles via SANS. 2. High Molecular Weight. *Macromolecules* **1991**, *24*, 2868-2876.
12. Casier, R.; Gauthier, M.; Duhamel, J. Using Pyrene Excimer Fluorescence to Probe Polymer Diffusion in Latex Films. *Macromolecules* **2017**, *50*, 1635-1644.
13. Hofmann, F. Process for Manufacturing Artificial Rubber. German patent 250690, September 12, 1909.
14. Gottlob, G. Caoutchouc Substance and Process of Making Same. U.S. Patent 1149577, January 6, 1913.
15. Mason, T.G.; Wilking, J.N.; Meleson, K.; Chang, C.B.; Graves, S.M. Nanoemulsions: Formation, Structure, and Physical Properties. *J. Phys.: Condens. Matter* **2006**, *18*, 635-666.

16. Karaman, M. E.; Meagher, L.; Pashley, R.M. Surface Chemistry of Emulsion Polymerization. *Langmuir*, **1993**, *9*, 1220-1227.
17. Mead, R.N.; Poehlein, G.W. Emulsion Copolymerization of Styrene-Methyl Acrylate and Styrene-Acrylonitrile in Continuous Stirred Tank Reactors. *Ind. Eng. Chem. Res.* **1988**, *27*, 2283-2293.
18. Li, B.; Brooks, B.W. Semi-batch Processes for Emulsion Polymerisation. *Polym. Int.* **1992**, *29*, 41-46.
19. SchoonBrood, H. A. S.; Thijssen, H. A.; Brouns, H. M.; Peters, M.; German, A. L. Semicontinuous Emulsion Copolymerization to Obtain Styrene-Methyl Acrylate Copolymers with Predetermined Chemical Composition Distributions. *J. Appl. Polym. Sci.* **1993**, *49*, 2029-2040.
20. Arzamendi, G.; Asua, J. M. Monomer Addition Policies for Copolymer Composition Control in Semicontinuous Emulsion Copolymerization. *J. Appl. Polym. Sci.* **1989**, *38*, 2019-2036.
21. Landfester, K. Miniemulsions for Nanoparticle Synthesis. *Top. Curr. Chem.* **2003**, *227*, 75-123.
22. Jackson, A.J. Introduction to Small-Angle Neutron Scattering and Neutron Reflectometry. **2008**. NIST Center for Neutron Research.
23. Yekta, A.; Duhamel, J.; Winnik, M. A. Dipole-Dipole Electronic Energy Transfer. Fluorescence Decay Functions for Arbitrary Distributions of Donors and Acceptors: Systems with Planar Geometry. *Chem. Phys. Lett.* **1995**, *235* 119-125.
24. Washington, I. Dynamic Modelling of Emulsion Polymerization for the Continuous Production of Nitrile Rubber. *University of Waterloo M.A.Sc. Thesis.* **2008**.
25. Gerrens, H. On Semicontinuous Emulsion Polymerization. *J. Polym. Sci. Part C.* **1969**, *27*, 77-93.
26. Wall, F. T.; Florin, R.E.; Delbecq, C. J. Copolymerization in Emulsion. *J. Am. Chem. Soc.* **1950**, *72*, 4769-4773.

27. Malmsten, M. Mobility of Biomolecules at Interfaces, *Biopolymers at Interfaces*. CRC Press: New York, **1998**, Volume 110, p. 249.
28. Thickett, S. C.; Gilbert, R. G. Emulsion Polymerization: State of the Art in Kinetics and Mechanisms. *Polymer*. **2007**, *48* 6965–6991.
29. Mayo, F.R.; Lewis, F. M. Copolymerization. I. A Basis for Comparing Behaviour of Monomers in Copolymerization; the Copolymerization of Styrene and Methylmethacrylate. *J. Am. Chem. Soc.* **1944**, *66*, 1594-1601.
30. Maxwell, I. A.; Aerdt, A. M.; German, A. L. Free Radical Copolymerization: An NMR Investigation of Current Kinetic Models. *Macromolecules*. **1993**, *26* 1956-1964.
31. Patino-Leal, H.; Reilly, P. M.; O'Driscoll, K. F. On the Estimation of Reactivity Ratios. *J. Polym. Sci. Part C*. **1980**, *18* 219-227.